~~CONFIDENTIAL~~

C.1

NACA

RESEARCH MEMORANDUM

FREE-FLIGHT INVESTIGATION OVER A MACH NUMBER RANGE FROM 0.74 TO 1.43 AT LIFT COEFFICIENTS FROM -0.15 TO 0.75 OF AN AIRPLANE-CONFIGURATION MODEL HAVING A 52.5° DELTA WING AND A LOW SWEPT HORIZONTAL TAIL

By Alan B. Kehlet

Langley Aeronautical Laboratory
Langley Field, Va.

NATIONAL ADVISORY COMMITTEE
FOR AERONAUTICS

WASHINGTON

September 28, 1956

~~CONFIDENTIAL~~

NACA RM L56G09

NATIONAL ADVISORY COMMITTEE FOR AERONAUTICS

RESEARCH MEMORANDUM

FREE-FLIGHT INVESTIGATION OVER A MACH NUMBER RANGE FROM 0.74 TO 1.43 AT LIFT COEFFICIENTS FROM -0.15 TO 0.75 OF AN AIRPLANE-CONFIGURATION MODEL HAVING A 52.5° DELTA WING AND A LOW SWEPT HORIZONTAL TAIL

By Alan B. Kehlet

SUMMARY

A free-flight investigation over a Mach number range of 0.74 to 1.43 at lift coefficients from -0.15 to 0.75 has been conducted to determine the aerodynamic characteristics of an airplane-configuration model having a 52.5° delta wing and a low, swept horizontal tail. The variations in lift-curve slopes and pitching-moment curves were nonlinear with lift coefficient over the lift range covered and increased with increasing lift coefficient. Near the same Mach number and lift coefficient that a similar configuration with a high-position horizontal tail pitched up, the model exhibited stable longitudinal stability characteristics. Good agreement of the present results was obtained with other experimental data and theory.

INTRODUCTION

As part of a general research program to investigate the longitudinal stability of wings having various plan forms and thickness ratios (ref. 1), a rocket-propelled model of an airplane configuration having a 52.5° delta wing and a low, swept all-movable horizontal tail has been flown.

The purpose of this test was to ascertain pitch-up characteristics, if any, of the present configuration at Mach numbers and lift coefficients where pitch-up occurred on a similar configuration with a high-position horizontal tail (ref. 2) and to determine lift, drag, and longitudinal stability at lift coefficients greater than those obtained from the test of reference 3.

The model used in the present investigation was the same in configuration as the model of reference 3 and was similar to the models of references 2, 4, and 5. Included in this paper are comparison figures of the experimental results obtained from the present investigation and the results of references 2, 3, 4, and 5. Theoretical and experimental comparisons of lift, drag, static longitudinal stability, horizontal-tail effectiveness, trim, and side-force derivative for the present test configuration are also included.

The model was flown at the Langley Pilotless Aircraft Research Station at Wallops Island, Va.

SYMBOLS

A_L longitudinal accelerometer reading, g units

A_N normal accelerometer reading, g units

A_T transverse accelerometer reading, g units

C_C chord-force coefficient, $-A_L\frac{W/S}{q}$

C_N normal-force coefficient, $A_{N_{cg}}\frac{W/S}{q}$

C_D drag coefficient, $C_C \cos \alpha + C_N \sin \alpha$

C_L lift coefficient, $C_N \cos \alpha - C_C \sin \alpha$

C_m pitching-moment coefficient about 0.28 mean aerodynamic chord

C_Y side-force coefficient, $A_T\frac{W/S}{q}$

$\bar{c}$ mean aerodynamic chord

g acceleration due to gravity, ft/sec^2

l horizontal-tail moment length, ft

M Mach number

M_X rolling moment

M_Y	pitching moment
M_Z	yawing moment
q	dynamic pressure, lb/sq ft; pitching velocity, radians/sec
S	total wing area (including area enclosed in fuselage), sq ft
t	time, sec
V	free-stream velocity, ft/sec
W	weight of model, lb
X	longitudinal body axis
Y	lateral body axis
Z	normal body axis
α	angle of attack, deg
$\dot{\alpha}$	time rate of change of angle of attack, $\frac{1}{57.3}\frac{\partial \alpha}{\partial t}$, radians/sec
β	angle of sideslip, deg
γ	flight-path angle, deg
δ	horizontal-tail deflection, deg
ϵ	inclination of principal axes, deg
θ	angle of pitch, radians
$\dot{\theta}$	time rate of change of angle of pitch, $\frac{\partial \theta}{\partial t}$, radians/sec
ϕ	angle of roll, radians
$\ddot{\phi}$	roll acceleration, $\frac{\partial^2 \phi}{\partial t^2}$, radians/sec^2
ψ	angle of yaw, deg

Derivatives

$C_{L_\alpha} = \frac{\partial C_L}{\partial \alpha}$, per deg

$C_{L_\delta} = C_{m_\delta} \frac{\bar{c}}{l}$

$C_{m_\alpha} = \left(\frac{\partial C_m}{\partial C_L}\right)_{trim} \left(C_{L_\alpha}\right)_{trim}$

$C_{m_{\dot{\alpha}}} = \frac{\partial C_m}{\partial \frac{\dot{\alpha}\bar{c}}{2V}}$

$C_{m_\delta} = C_{m_{\alpha_{av}}} \left(\frac{\Delta\alpha}{\Delta\delta}\right)_{trim}$

$C_{m_q} = \frac{\partial C_m}{\partial \frac{q\bar{c}}{2V}}$

$C_{Y_\beta} = \frac{\partial C_Y}{\partial \beta}$

Subscripts:

a	aileron
cg	center of gravity
e	elastic or elevator
F	fuselage
I	interference
r	rigid
T	tail
W	wing

The system of body axes and the positive values of control deflection, forces, moments, and angles are shown in figure 1.

MODEL

A three-view drawing of the model is shown in figure 2. Photographs of the model are shown in figure 3.

The empennage and fuselage are described in references 6 and 7, respectively. The steel delta wing is described in reference 3, briefly however; the wing had 52.5° leading-edge sweep, a taper ratio of zero, and NACA 65A003 airfoil sections in the streamwise direction.

Each panel of the horizontal tail was deflected in an approximately square-wave program by a separate servocontrol fed by a common pressure system and regulated by an electric motor-driven selector valve. For the present investigation, the stop positions were approximately -1.0° and -5.0° measured in a plane parallel to the fuselage plane of symmetry.

The model weighed 132.25 pounds and had moments of inertia in pitch, yaw, and roll of 8.51, 8.68, and 0.42 slug-ft^2, respectively. Inclination of the principal axis was not measured but was estimated from measurements of similar configurations to be 0.5° below the body axis at the nose. The product of inertia due to the inclination of the principal axis was 0.07 slug-ft^2. The center of gravity was at a station corresponding to 0.28 of the wing mean aerodynamic chord.

As stated before, the model in the present investigation was the same in configuration as the model of reference 3. Differences were in mass characteristics and construction of the vertical tail. The present model had a solid aluminum-alloy vertical tail, whereas the model of reference 3 had a wood—aluminum-alloy laminated vertical tail.

INSTRUMENTATION

The model was equipped with an NACA telemetering system which transmitted continuous measurements of normal acceleration at the center of gravity, normal acceleration at a nose reference station, angle of attack, angle of sideslip, longitudinal acceleration, transverse acceleration, roll acceleration, control position of one panel of the horizontal tail, total pressure, and reference static pressure.

Flight-path information and atmospheric conditions at altitude were obtained from a correlation of reference static-pressure, total-pressure, and radiosonde data; the radiosonde was released immediately after the flight.

The reference static-pressure orifice was located on top of the model about 0.7 body diameter behind the forward station of the cylindrical part of the body. This pressure orifice has been calibrated against true free-stream static pressure during tests of several models flown in this general program and has been used, in this test, to determine free-stream static pressure throughout the flight.

FLIGHT TEST AND ANALYSIS

Flight Test

The model was launched at an angle of approximately 60° from the horizontal by means of a mobile launcher as shown in figure 3(b). A single 6-inch-diameter solid-fuel ABL Deacon rocket motor boosted the model to maximum velocity.

Analysis

The response of the model in the longitudinal mode to deflections of an all-movable horizontal tail in an approximately square-wave program is usually analyzed by a method such as reference 7 which assumes, essentially, two degrees of freedom.

In the present investigation, however, because the two horizontal-tail panels are mechanically independent of each other and, therefore, do not necessarily deflect simultaneously nor have the same stop positions, lateral motions were induced throughout the flight. The lateral motions were generally not negligible so that the two-degree-of-freedom method was not believed entirely applicable. Presented in figure 4 as a function of Mach number are the variations of C_{m_α} as obtained from the two-accelerometer method (described in ref. 8) and the two-degree-of-freedom (period) method.

Over the Mach number range covered, generally the period method resulted in a higher degree of static stability than the two-accelerometer method. Studies made in reference 4 indicate that violation of the two-degree-of-freedom assumptions primarily affects the period and damping; thus, in the present investigation, the two-accelerometer method is believed to give a better indication of static stability and is therefore used to determine the static-stability parameters presented in the results. The rotary-damping derivatives $\left(C_{m_q} + C_{m_{\dot{\alpha}}}\right)$ as determined from the two-degree-of-freedom method are not presented but were generally in the range of -10 to -15 throughout the Mach number range.

As explained in more detail in reference 4, it is believed that as long as the instruments are properly corrected for position (that is, position in the model) to the center-of-gravity position, the angle of attack, normal force, and chord force can be measured, regardless of coupling, with as much accuracy as in cases of pure longitudinal motions.

CORRECTIONS AND ACCURACY

Measured quantities obtained from the instrumentation were corrected for instrument position off the center of gravity. Corrections for model pitching and yawing velocities were also made by the method of reference 9 to the readings of the air-flow indicator to obtain angles of attack and angles of sideslip. Indicated accelerations were corrected to accelerations at the center of gravity.

In most cases with rocket-propelled model instrumentation, corrections for instrument frequency response are negligible; however, the roll angular accelerometer used in the present investigation did have an appreciable phase lag (about 15° at $M = 1.3$). The data presented from this instrument were not corrected for phase lag. It also should be pointed out that the absolute magnitude of the roll-angular-accelerometer data may be in error by as much as 25 percent throughout the Mach number range.

Because instruments cannot be calibrated during and after flight, the absolute accuracy of the measured quantities is impossible to establish. Since CW Doppler radar is believed to be in error by less than 1 percent and peak velocity was determined by a CW Doppler radar set, peak Mach number should be accurate to about ± 1 percent. Mach number subsequent to peak was determined from model instrumentation and is believed to be accurate to about ± 3 percent at $M = 0.80$. An indication of the systematic instrument errors possible is given by the following table, based on an accuracy of ± 1 percent of the full instrument range. Coefficient errors due to dynamic-pressure inaccuracies are included.

M	C_N	C_C	C_Y
1.4	±0.007	±0.001	±0.003
.8	±.029	±.007	±.014

An indication of random errors encountered may be noted from the scatter of data points shown in the figures. Errors in angle of attack and control-panel deflection are independent of dynamic pressure and

are not likely to vary with Mach number. The horizontal-tail deflections are estimated to be accurate within $\pm 0.10^{\circ}$ and trim angles of attack within $\pm 0.50^{\circ}$.

RESULTS AND DISCUSSION

The variations of dynamic pressure and Reynolds number (based on wing mean aerodynamic chord) with Mach numbers are shown in figure 5. The dynamic pressure and Reynolds number range covered were from about 600 to 2,900 lb/sq ft and about 5.1×10^6 to 11.9×10^6, respectively.

Time History

A time history of some of the quantities measured in the present investigation is shown in figure 6. Throughout the flight, the model exhibited oscillations in the lateral mode when pulsed primarily in pitch. These lateral oscillations are believed to be the result of a lateral input from the two horizontal-tail panels not pulsing simultaneously. (On fig. 6, note the large rolling accelerations occurring each time the tail panels are moved.) The lateral oscillations are generally of appreciable magnitude (although exaggerated by the scales of fig. 6), particularly at supersonic speeds, and coupling of motions is probably present throughout the Mach number range.

Longitudinal Trim

The variations of the trim lift coefficient and trim angle of attack at the two tail settings as functions of Mach number as obtained from the present test and the test of reference 3 are shown in figure 7. Although about 2-percent mean-aerodynamic-chord center-of-gravity-location difference exists between the two models, the primary reason for the different levels of trim is the horizontal-tail settings.

The model in the present test covered a trim lift-coefficient range of about 0.1 to 0.5 at subsonic speeds and of about 0 to 0.2 at the maximum Mach number at $\delta = -1.0^{\circ}$ and $\delta = -5.0^{\circ}$, respectively. Throughout the Mach number range for both the present test and the test of reference 3, trim changes at both tail settings were moderate and without sharp breaks.

Lift

The variation of the lift coefficient with angle of attack at the two tail settings for both the present test and the test of reference 3 is shown in figure 8. It can be seen from the data that the lift-curve slopes vary nonlinearly with lift coefficient. At $M = 0.79$ and 0.86 and at $C_L = 0.5$, two different values of C_{L_α} from the same oscillation

may be obtained. The reason for the different slopes is not known; however, it may be due to wing flow separation. The agreement between the two tests is good.

Lift-curve slopes represented by the faired lines in figure 8 at $C_L = 0$ and 0.3 are presented as functions of Mach number in figure 9. The agreement between the two tests is excellent. In this figure also it is evident that C_{L_α} does not vary linearly with C_L with the higher value of C_{L_α} at $C_L = 0.3$. Two factors are believed responsible for this type of nonlinear variation; wing-alone data (ref. 10) show a similar nonlinearity and the increase of lift on the horizontal tail with angle of attack as the tail moves out of the main downwash flow field.

Also included in figure 9 are lift-curve slopes for a wing-body-tail configuration and a wing-body combination from wind-tunnel data (refs. 11 and 12, respectively). The agreement among the four tests is very good considering the differences in configuration and that the wind-tunnel slopes are average values over a lift-coefficient range of about -0.10 to 0.35.

Drag

The variation of drag coefficient with lift coefficient at the various average Mach numbers is shown in figure 10. It should be pointed out that drag coefficients were computed with sideslip and side-force effects neglected. Calculations showed that these effects were small. The data from reference 3 are not presented as a comparison since it is believed that the reference model had a misalinement of the longitudinal accelerometer such that a component of the normal force reduced the chord force as angle of attack was increased. When the discrepancy between the two models was noted, a check was made of chord force against angle of attack, and the reference model exhibited an apparent leading-edge suction far in excess of what normally would be expected. For this reason, no comparison of drag polars between the two models is presented.

The minimum drag coefficients are presented as a function of Mach number in figure 11. Since the lift coefficient for minimum drag was near zero at all Mach numbers for the present test and the test of reference 3 and since, therefore, accelerometer misalinement would have only a negligible effect, comparisons are presented. As with the lift-curve slopes, the agreement between the two tests in both drag level and drag rise is very good. Values of the minimum drag coefficient increased from about 0.015 at subsonic speeds to a maximum of about 0.034 at $M = 1.10$ and from thereon decreased with increasing Mach number.

The maximum lift-drag ratios and the lift coefficients at which $(L/D)_{max}$ occurs are shown as a function of Mach number in figure 12. The maximum lift-drag ratio decreased from about 7.4 at $M = 0.80$ to about 4.4 at $M = 1.40$; lift coefficients corresponding to these values are about 0.27 and 0.30, respectively.

Longitudinal Static Stability

As mentioned previously, the model in the present test exhibited motions in both the longitudinal and lateral modes; because of the motions in the lateral mode, the two-degree-of-freedom method of analysis is not believed to be entirely applicable. For reasons mentioned in the section entitled "Analysis," the two-accelerometer method of obtaining instantaneous total pitching moments was used in preference to the two-degree-of-freedom period method. The pitching-moment coefficients presented herein are total; that is, they include the rotary damping term $C_{m_q} + C_{m_{\dot{\alpha}}}$. When a value of $C_{m_q} + C_{m_{\dot{\alpha}}}$ greater than that determined from the two-degree-of-freedom method was used, the effect of the rotary damping on C_m was determined for a typical oscillation; no change in slope was noted.

The variation of the total pitching-moment coefficient with lift coefficient at the two tail settings is shown in figure 13. At subsonic Mach numbers and the high-lift tail setting, the slope of the pitching-moment curve increases negatively with increasing lift coefficient over the lift range covered. As stated previously one of the purposes of the present test was to ascertain the static stability of a low-position horizontal-tail model at conditions where pitch-up occurred on a similar configuration with the horizontal tail mounted in a high position. Presented in figure 14 are the pitching-moment-curve results from the present test and the tests of references 2, 4, and 5 at Mach numbers from 0.90 to 0.95. At positive lift coefficients, the low-tail models show no unstable breaks in the pitching-moment curves. The diamond-plan-form wing-model results of reference 5 are included to show the effect that negative lift coefficients have on the pitching moments with a low horizontal tail. A low-tail model exhibits similar characteristics at negative lift coefficients as a high-tail model at positive lift coefficients. The difference in stability characteristics of the two tail-position models at positive lift coefficients is consistent with the thought of downwash effects on the tail either increasing or decreasing (high or low tail position, respectively) as lift coefficient is increased.

The variation of the static-stability parameter $\partial C_m/\partial C_L$ with Mach number measured at trim conditions for both the present test and test of reference 3 is shown in figure 15. At supersonic Mach numbers, both models exhibit about the same stability even though there exists a difference in trim and a slight difference in center-of-gravity location.

At subsonic Mach numbers, however, the increase in static stability with increased lift coefficient becomes apparent, with the present test (at $\delta = -5.0^\circ$), exhibiting greater stability than the test of reference 3.

The variation of the ability of the horizontal tail to produce lift and the effectiveness in producing moment as a function of Mach number is shown in figure 16. Also included in this figure are the data of reference 3. Good agreement is obtained at supersonic speeds. At subsonic speeds, however, since C_{L_δ} and C_{m_δ} were obtained from $\partial C_m/\partial C_L$, the difference in static stability between the two models is reflected in the values of C_{L_δ} and C_{m_δ} with the model in the present test exhibiting the greater values.

Side-Force Characteristics

The variation of side-force coefficient with angle of sideslip at low angles of sideslip is shown in figure 17. The slopes of the curves of C_Y against β, as represented by the faired lines in figure 17, are presented as a function of Mach number in figure 18. The shape of the curve of C_{Y_β} with Mach number (almost constant) is similar to the variation of a 60° sweptback-wing lift-curve slope with Mach number (ref. 13), and most of the side force associated with angle of sideslip is believed to be due to the vertical tail. Because of the motions present in both pitch and yaw, yawing-moment coefficient obtained from the measured lateral periods is not presented.

Theoretical Comparisons

Theoretical studies of lift, static longitudinal stability, trim, drag, and lateral-force derivatives as functions of Mach number have been made for a tail setting of -1.0° and are presented with experimental results for comparison. The experimental data presented in this section have been corrected for wing, horizontal-tail and vertical-tail flexibility by a method described in reference 8. The data of reference 3 (same model configuration) have been used in this section to extend the Mach number range of the present test from 1.4 to 1.8; for example, at Mach numbers greater than 1.4, the values of $C_{L_{\alpha_{trim}}}$ were assumed to be the same as the values of C_{L_α} at $C_L = 0$. Similarly, the values of dynamic pressure used in calculating flexibility corrections at Mach numbers greater than 1.4 were assumed to be approximately the values of q from reference 3.

The variations of experimental and theoretical results of C_L against α and of C_m against C_L at Mach numbers near 0.80 and 1.40 for the complete configuration are shown in figure 19. Theoretical values were calculated from the theory of reference 14. This theory predicts an accuracy of ±10 percent for lift-curve slope and ±0.02 of the body length for center-of-pressure positions for most wing-body-tail combinations throughout a Mach number range of 0.20 to 2.0. It can be seen that the predicted accuracy for slopes at the two Mach numbers is realized although the values of α and C_m at $C_L = 0$ are in only fair agreement. Correcting the experimental results for flexibility improves slope agreement with theoretical values.

The variation of flexible to rigid lift ratios is shown in figure 20 as a function of Mach number. The configuration exhibited from about 97 percent at $M = 0.75$ to 90 percent at $M = 1.80$ of the rigid values of lift-curve slope.

Presented in figures 21, 22, 23, 24, and 25 are the variations of theoretical and experimental values of lift-curve slope, static longitudinal stability parameters, horizontal-tail effectiveness, and trim data as functions of Mach number. Theoretical values were calculated by using the theories of references 14, 15, and 16.

All comparisons indicate from fair agreement at subsonic speeds to good agreement at supersonic speeds and are generally within the predicted accuracy of the theory. It should be pointed out that the experimental lift-curve slopes presented were taken at $C_{L_{trim}}$ conditions and corrected for flexibility. Theoretical lift-curve slopes of exposed wing plus interference (theory of ref. 15) are included since this theory has given good agreement with previous experimental results. Theoretical pitching-moment results are generally not in as good agreement with experimental results as lift-curve slopes but are well within the accuracy of ±0.02 body length claimed by reference 14. Experimental trim characteristics were computed from rigid experimental pitching-moment values by assuming that the pitching moment at zero tail setting and angle of attack was zero. Data of reference 1 indicate that for a similar configuration the value of C_m at zero tail setting and zero angle of attack is approximately zero.

The variation of experimental and theoretical drag coefficient as a function of Mach number is shown in figure 26. The theoretical drag curves were obtained from reference 17, where a drag analysis of the configuration tested was made. Good agreement of subsonic and supersonic levels of drag coefficient was obtained.

Presented in figure 27 are the theoretical and experimental values of side-force derivative. Theories of references 18 and 19 were used to calculate the theoretical values. The results are in good agreement.

CONCLUSIONS

A free-flight investigation of the aerodynamic characteristics at transonic and supersonic speeds of an airplane configuration having a 52.5° delta wing and a low, swept horizontal tail indicates the following conclusions:

1. Throughout the flight, the model oscillated in both the longitudinal and lateral modes. Coupling of the motions between the two modes was believed to be present.

2. The lift-curve slopes were nonlinear with a higher value of lift-curve slope at a lift coefficient of 0.3 than at a lift coefficient of 0.

3. The maximum lift-drag ratios decreased from about 7.4 near a Mach number of 0.80 to about 4.4 at a Mach number of 1.4 with corresponding lift coefficients of about 0.27 and 0.30, respectively.

4. At near the same Mach number and lift coefficient at which pitch-up occurred on a similar configuration with the horizontal tail mounted in the high position, the model exhibited stable static-stability characteristics.

Langley Aeronautical Laboratory,
National Advisory Committee for Aeronautics,
Langley Field, Va., June 21, 1956.

REFERENCES

1. McFall, John C., Jr.: Longitudinal Stability Investigation for a Mach Number Range of 0.8 to 1.7 of an Airplane Configuration With a 45° Swept Wing and a Low Horizontal Tail. NACA RM L55L09, 1956.

2. Peck, Robert F., and Mitchell, Jesse L.: Rocket-Model Investigation of Longitudinal Stability and Drag Characteristics of an Airplane Configuration Having a 60° Delta Wing and a High Unswept Horizontal Tail. NACA RM L52K04a, 1953.

3. Kehlet, Alan B.: Aerodynamic Characteristics at Transonic and Supersonic Speeds of a Rocket-Propelled Airplane Configuration Having a 52.5° Delta Wing and a Low, Swept Horizontal Tail. NACA RM L54A20, 1954.

4. Peck, Robert F., and Coltrane, Lucille C.: Longitudinal Characteristics at Transonic and Supersonic Speeds of a Rocket-Propelled Airplane Model Having a 60° Delta Wing and a Low Swept Horizontal Tail. NACA RM L55F27, 1955.

5. Kehlet, Alan B.: Aerodynamic Characteristics at Transonic and Supersonic Speeds of a Rocket-Propelled Airplane Configuration Having a Diamond-Plan-Form Wing of Aspect Ratio 3.08 and a Low, Swept Horizontal Tail. NACA RM L54G27a, 1954.

6. McFall, John C., Jr.: Longitudinal Stability Characteristics at Transonic Speeds of a Rocket-Propelled Model of an Airplane Configuration Having a 45° Swept Wing of Aspect Ratio 6.0. NACA RM L53G22a, 1954.

7. Gillis, Clarence L., Peck, Robert F., and Vitale, A. James: Preliminary Results From a Free-Flight Investigation at Transonic and Supersonic Speeds of the Longitudinal Stability and Control Characteristics of an Airplane Configuration With a Thin Straight Wing of Aspect Ratio 3. NACA RM L9K25a, 1950.

8. Vitale, A. James: Effects of Wing Elasticity on the Aerodynamic Characteristics of an Airplane Configuration Having 45° Sweptback Wings As Obtained From Free-Flight Rocket-Model Tests at Transonic Speeds. NACA RM L52L30, 1953.

9. Mitchell, Jesse L., and Peck, Robert F.: An NACA Vane-Type Angle-of-Attack Indicator for Use at Subsonic and Supersonic Speeds. NACA TN 3441, 1955. (Supersedes NACA RM L9F28a.)

10. Few, Albert G., Jr., and Fournier, Paul G.: Effects of Sweep and Thickness on the Static Longitudinal Aerodynamic Characteristics of a Series of Thin, Low-Aspect-Ratio, Highly Tapered Wings at Transonic Speeds - Transonic-Bump Method. NACA RM L54B25, 1954.

11. Tinling, Bruce E., and Lopez, Armando E.: The Effects of Horizontal-Tail Location and Size on the Subsonic Longitudinal Aerodynamic Characteristics of an Airplane Model Having a Triangular Wing of Aspect Ratio 3. NACA RM A53L15, 1954.

12. Heitmeyer, John C.: Effect of Vertical Position of the Wing on the Aerodynamic Characteristics of Three Wing-Body Combinations. NACA RM A52L15a, 1953.

13. Vitale, A. James, McFall, John C., Jr., and Morrow, John D.: Longitudinal Stability and Drag Characteristics at Mach Numbers From 0.75 to 1.5 of an Airplane Configuration Having a 60° Swept Wing of Aspect Ratio 2.24 As Obtained From Rocket-Propelled Models. NACA RM L51K06, 1952.

14. Nielsen, Jack N., Kaattari, George E., and Anastasio, Robert F.: A Method for Calculating the Lift and Center of Pressure of Wing-Body-Tail Combinations at Subsonic, Transonic, and Supersonic Speeds. NACA RM A53G08, 1953.

15. Tucker, Warren A.: A Method for Estimating the Components of Lift of Wing-Body Combinations at Supersonic Speeds. NACA RM L52D22, 1952.

16. DeYoung, John, and Harper, Charles W.: Theoretical Symmetric Span Loading at Subsonic Speeds for Wings Having Arbitrary Plan Form. NACA Rep. 921, 1948.

17. Holdaway, George H., and Mersman, William A.: Application of Tchebichef Form of Harmonic Analysis to the Calculation of Zero-Lift Wave Drag of Wing-Body-Tail Combinations. NACA RM A55J28, 1956.

18. Sacks, Alvin H.: Aerodynamic Forces, Moments, and Stability Derivatives for Slender Bodies of General Cross Section. NACA TN 3283, 1954.

19. Heaslet, Max A., Lomax, Harvard, and Jones, Arthur L.: Volterra's Solution of the Wave Equation As Applied to Three-Dimensional Supersonic Airfoil Problems. NACA Rep No. 889, 1947. (Supersedes NACA TN 1412.)

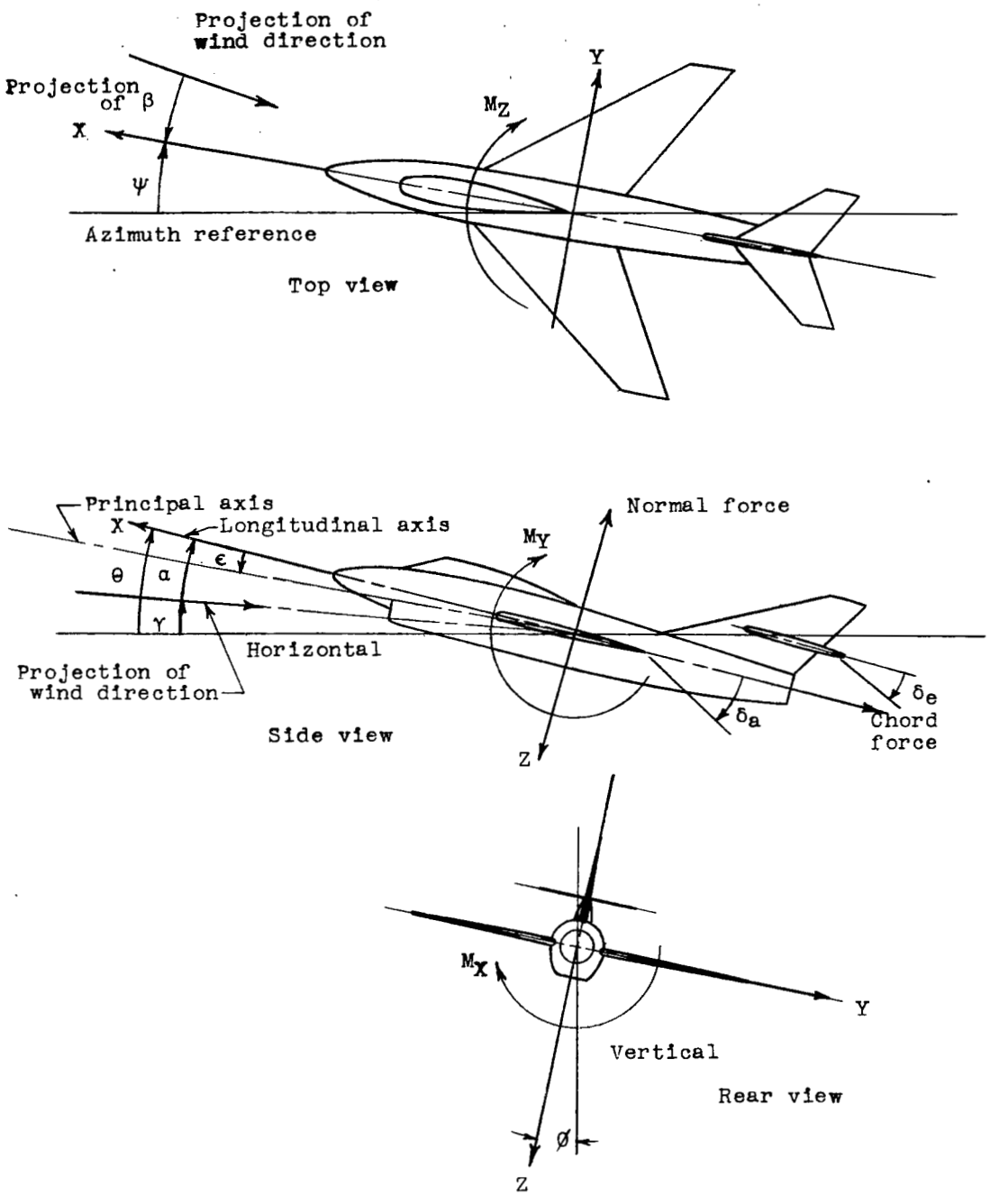

Figure 1.- System of body axes and angular relationships. Each view presents a plane of the axes system as viewed along and in a positive direction of the third axis.

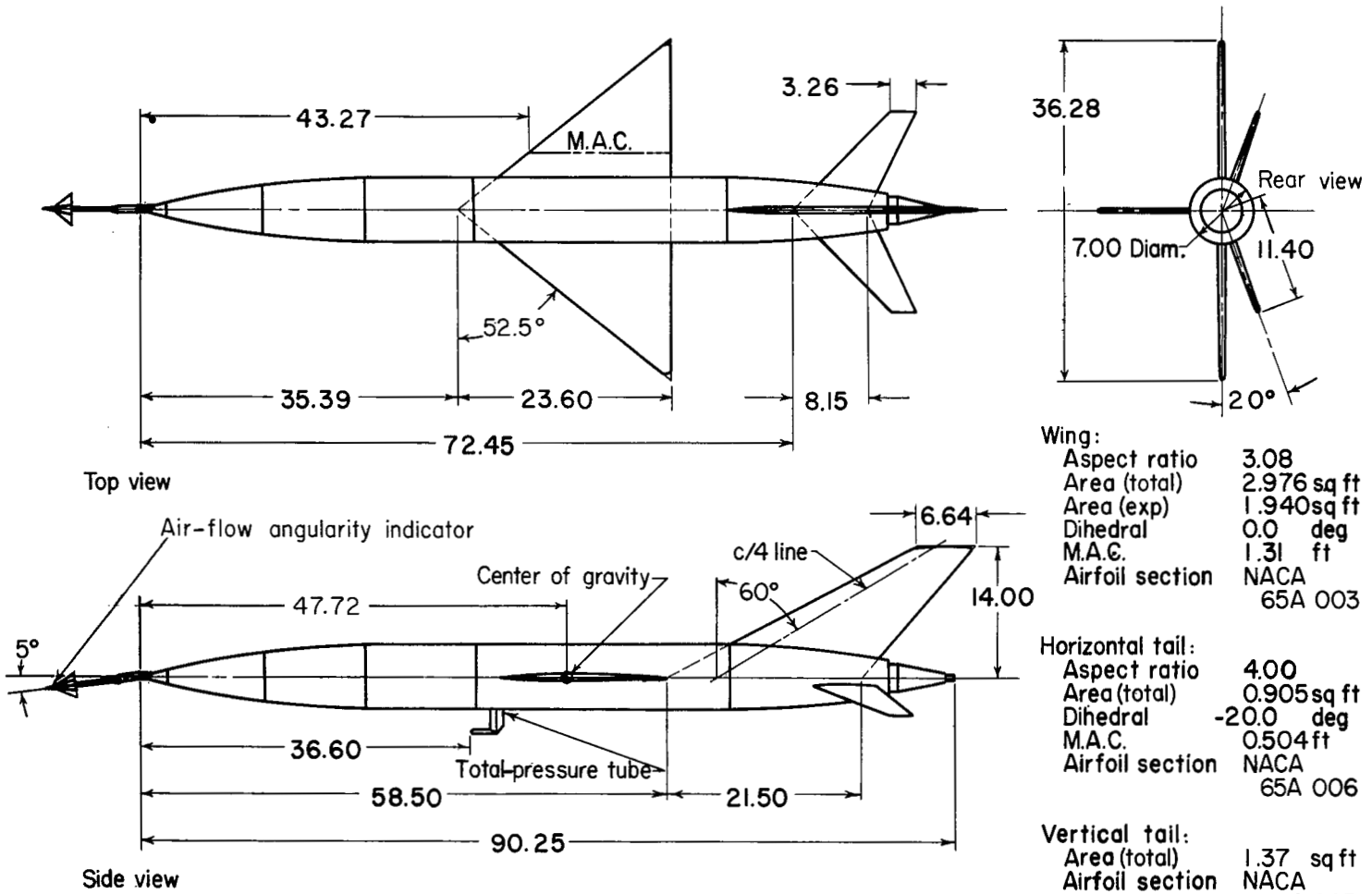

Figure 2.- General arrangement of model. All dimensions are in inches.

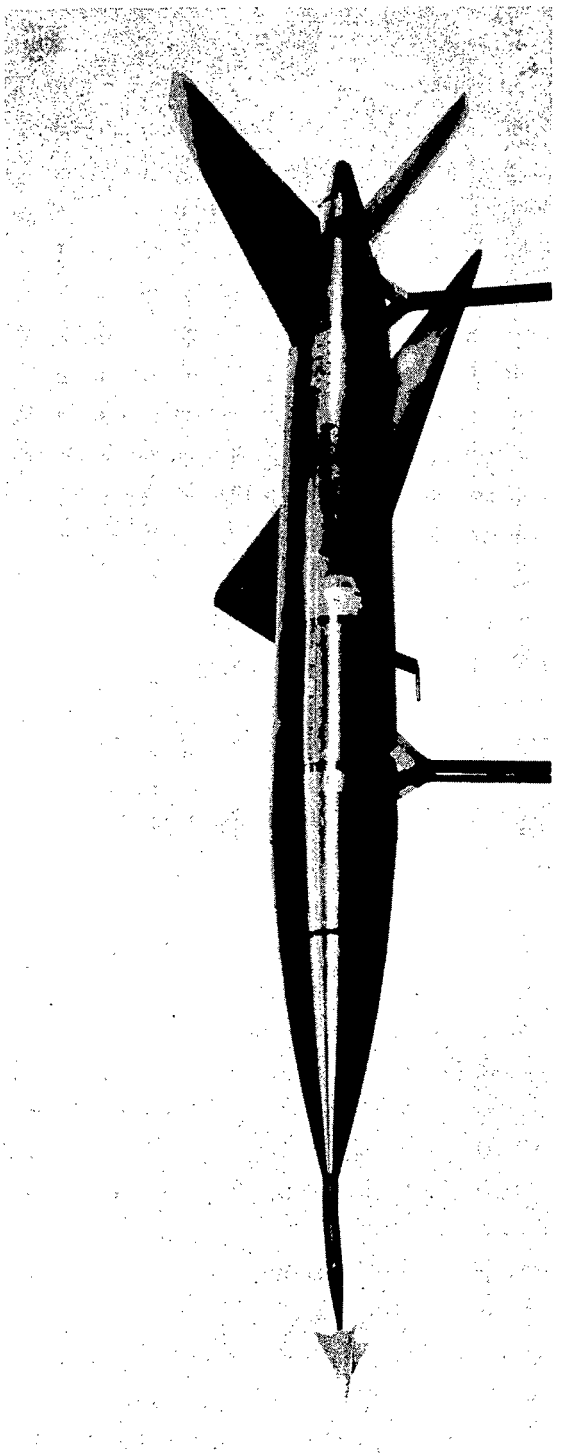

L-85511

(a) Three-quarter front view.

Figure 3.- Photographs of model.

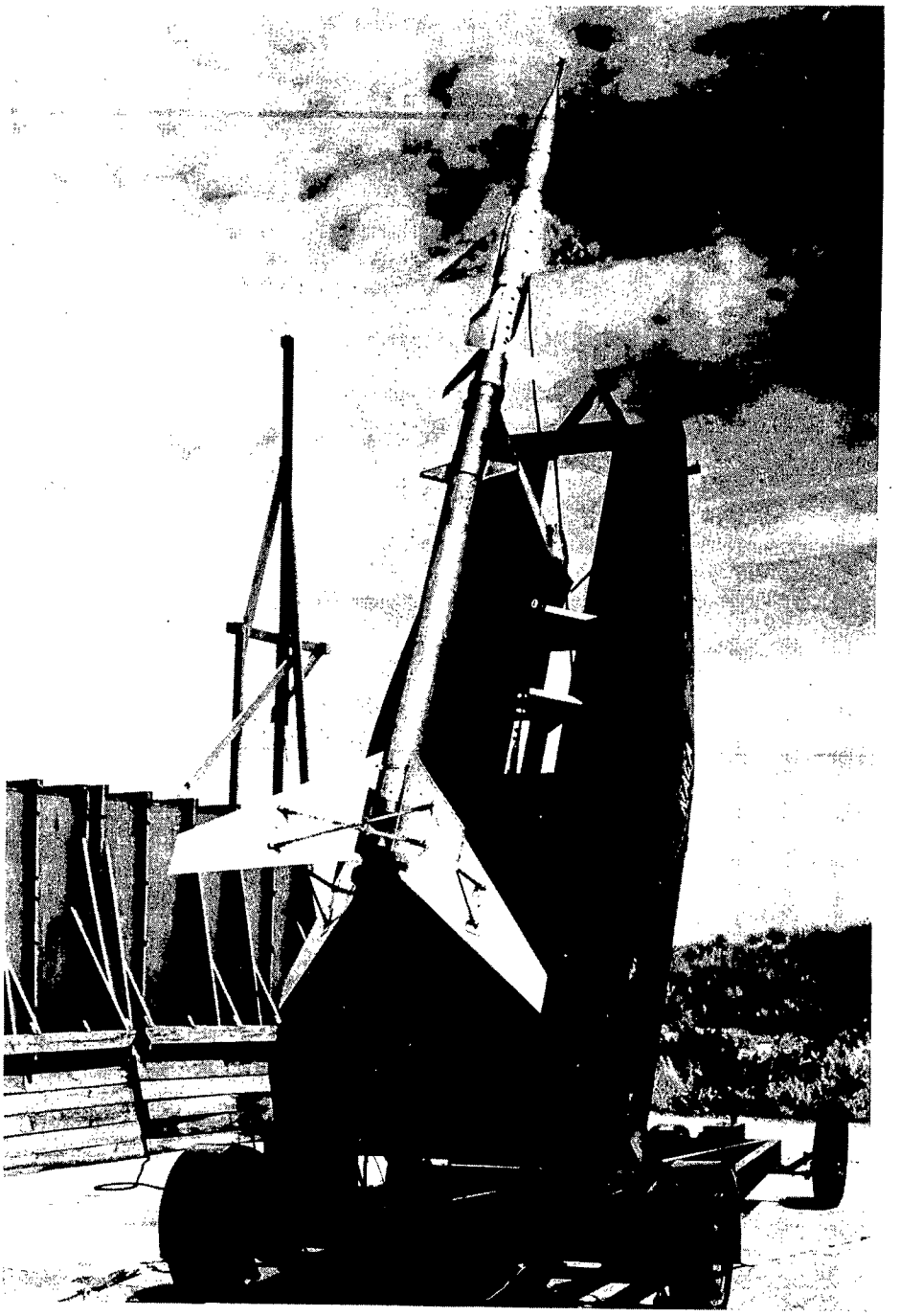

L-85763.1

(b) Model on launcher.

Figure 3.- Concluded.

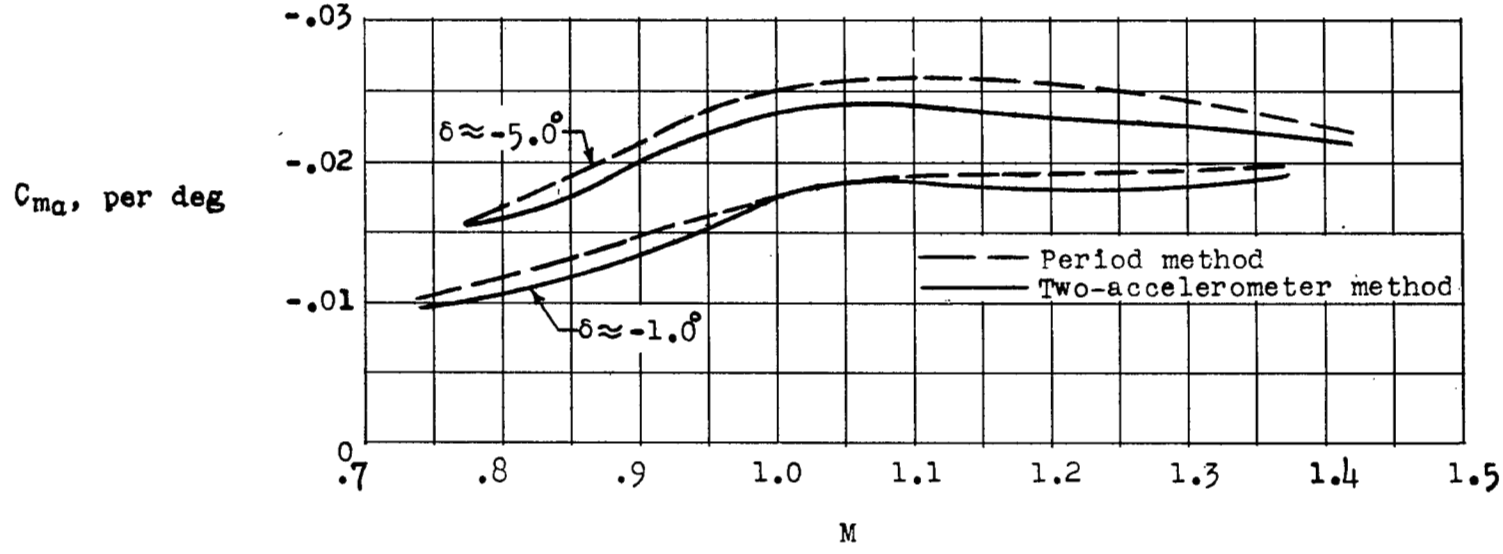

Figure 4.- Variation of static-stability parameter C_{m_α} with Mach number.

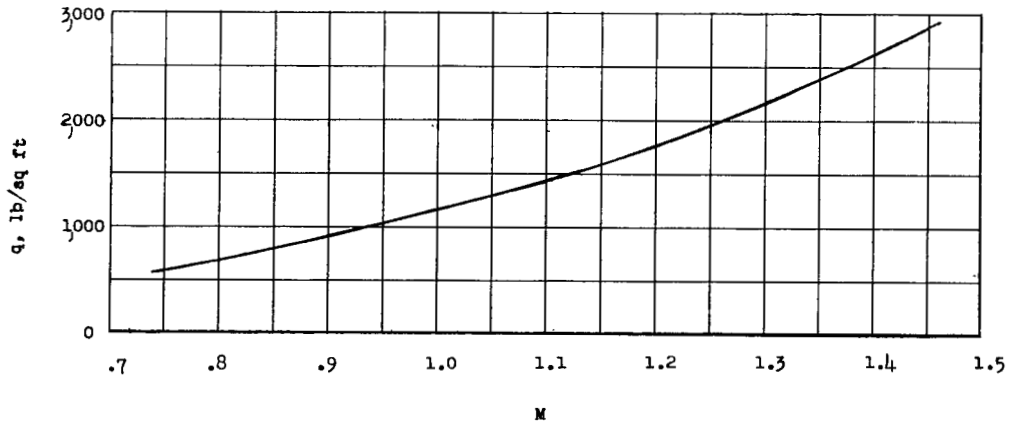

(a) Dynamic pressure.

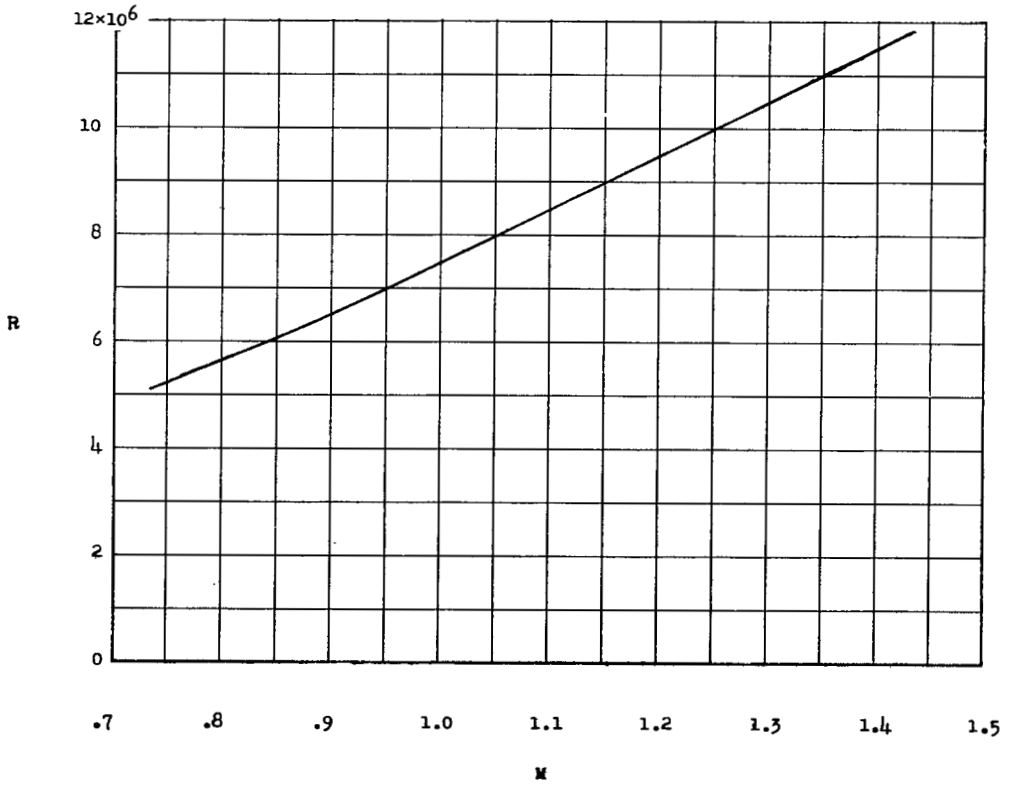

(b) Reynolds number.

Figure 5.- Variation of dynamic pressure and Reynolds number with Mach number.

(a) Supersonic Mach numbers.

Figure 6.- Time history of some of the quantities measured in present investigation.

(b) Subsonic Mach numbers.

Figure 6.- Concluded.

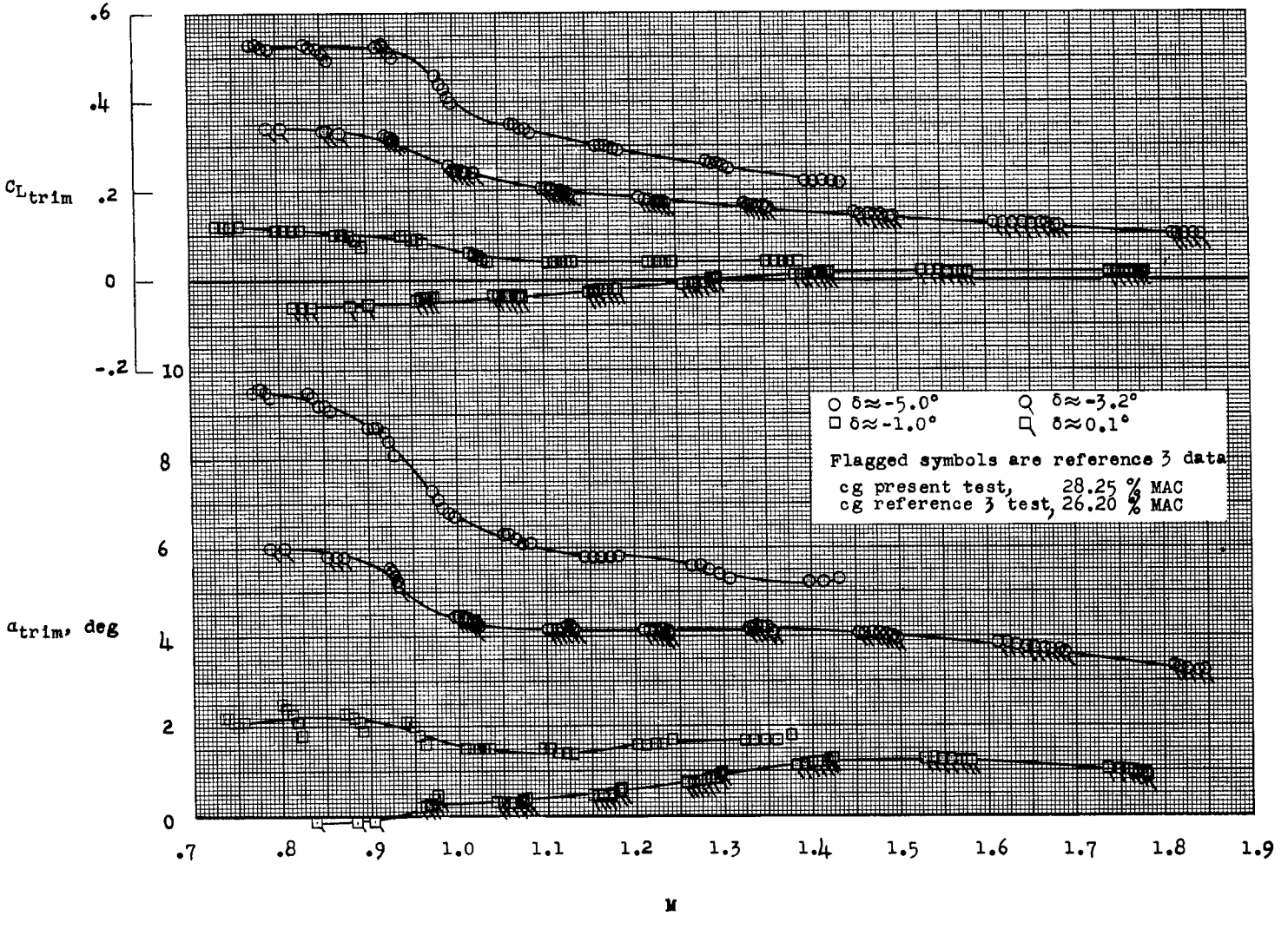

Figure 7.- Variation of longitudinal trim characteristics with Mach number.

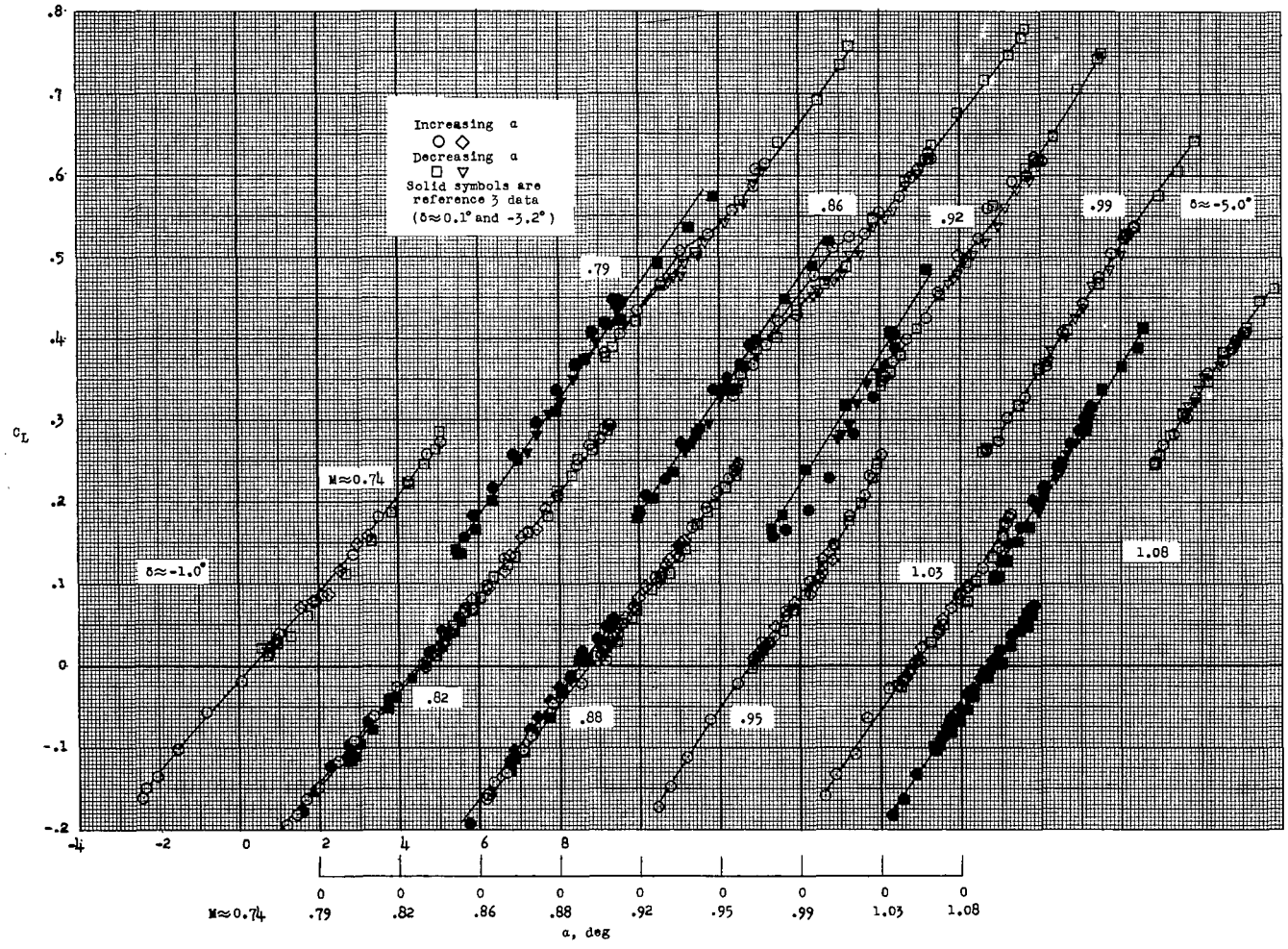

(a) Transonic Mach numbers.

Figure 8.- Variation of lift coefficient with angle of attack at transonic and supersonic Mach numbers.

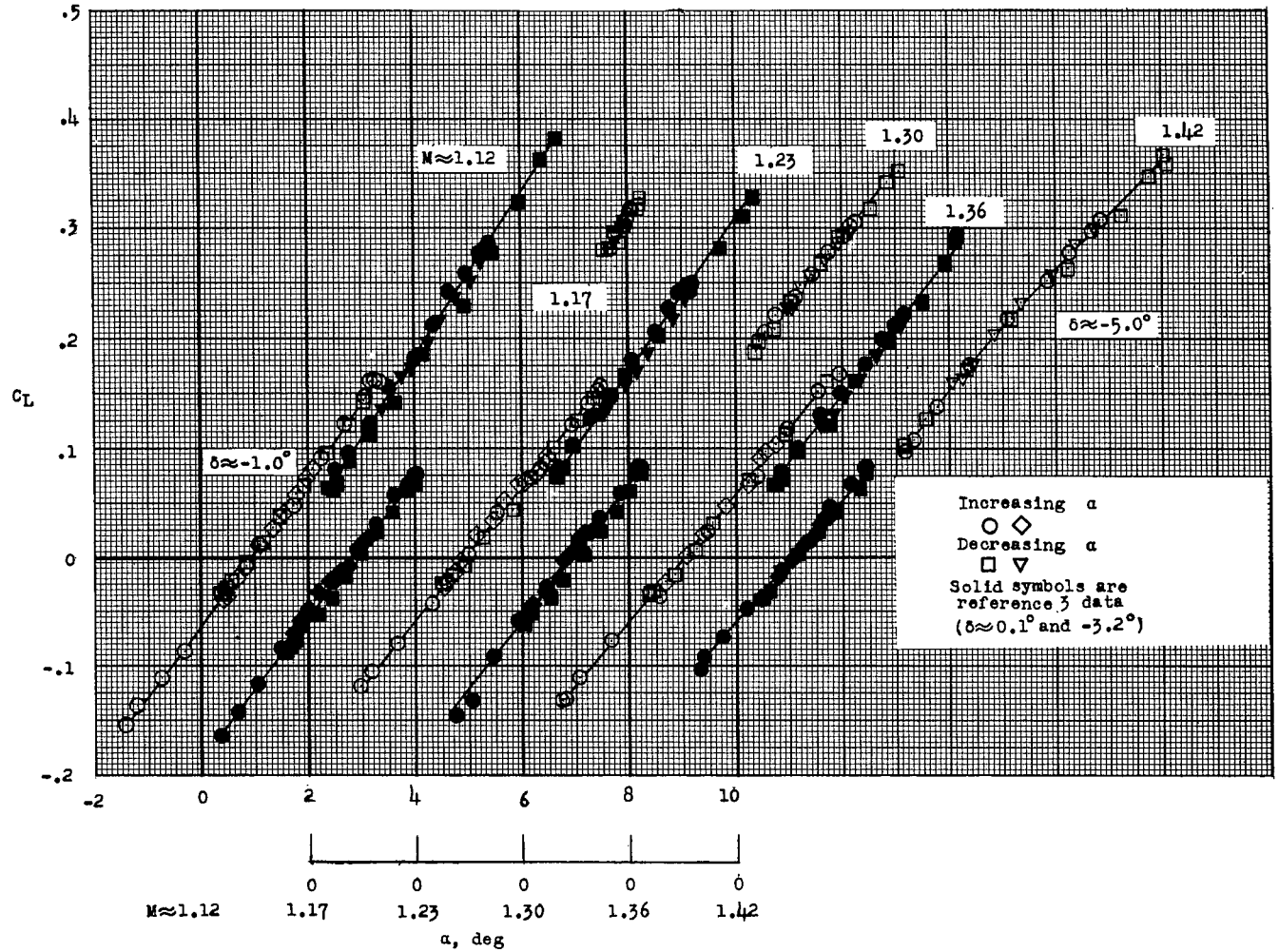

(b) Supersonic Mach numbers.

Figure 8.- Concluded.

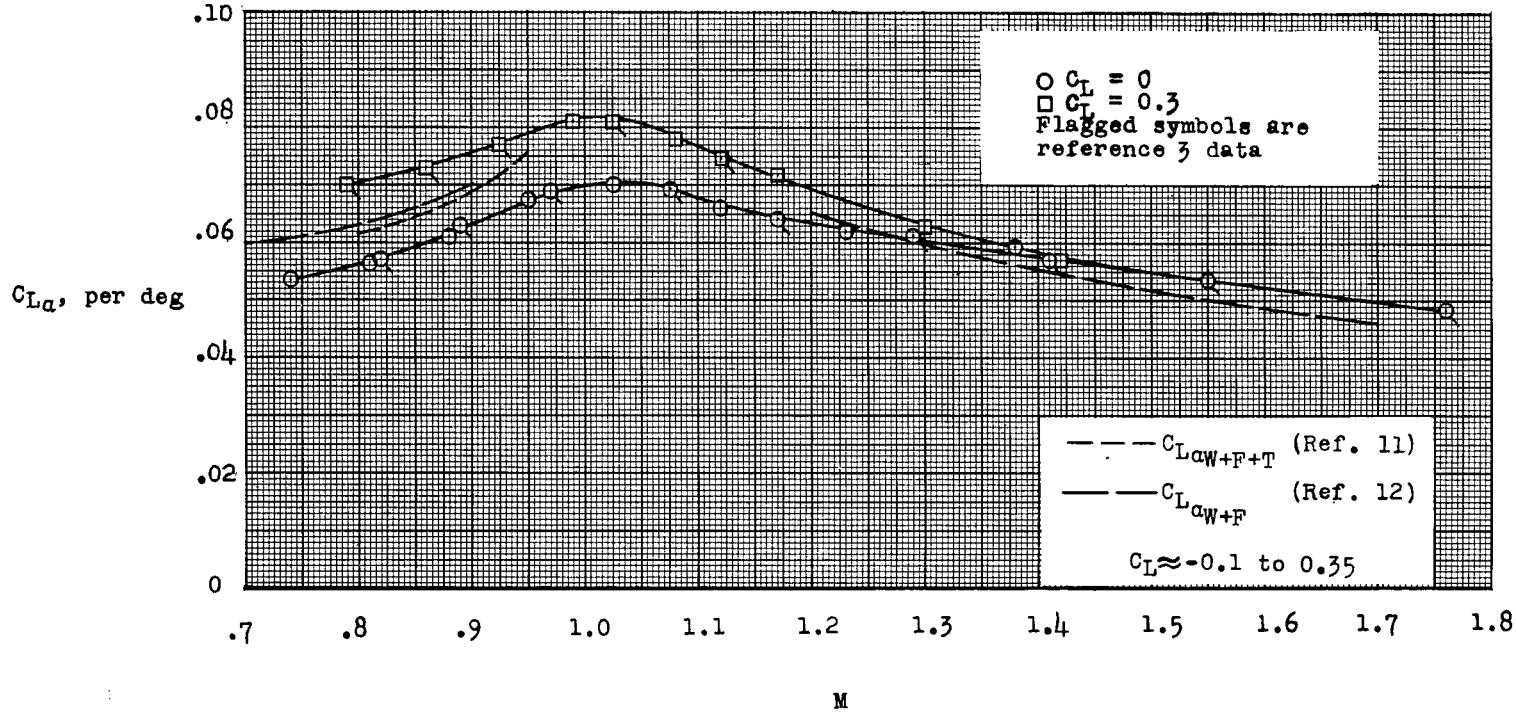

Figure 9.- Variation of lift-curve slope with Mach number.

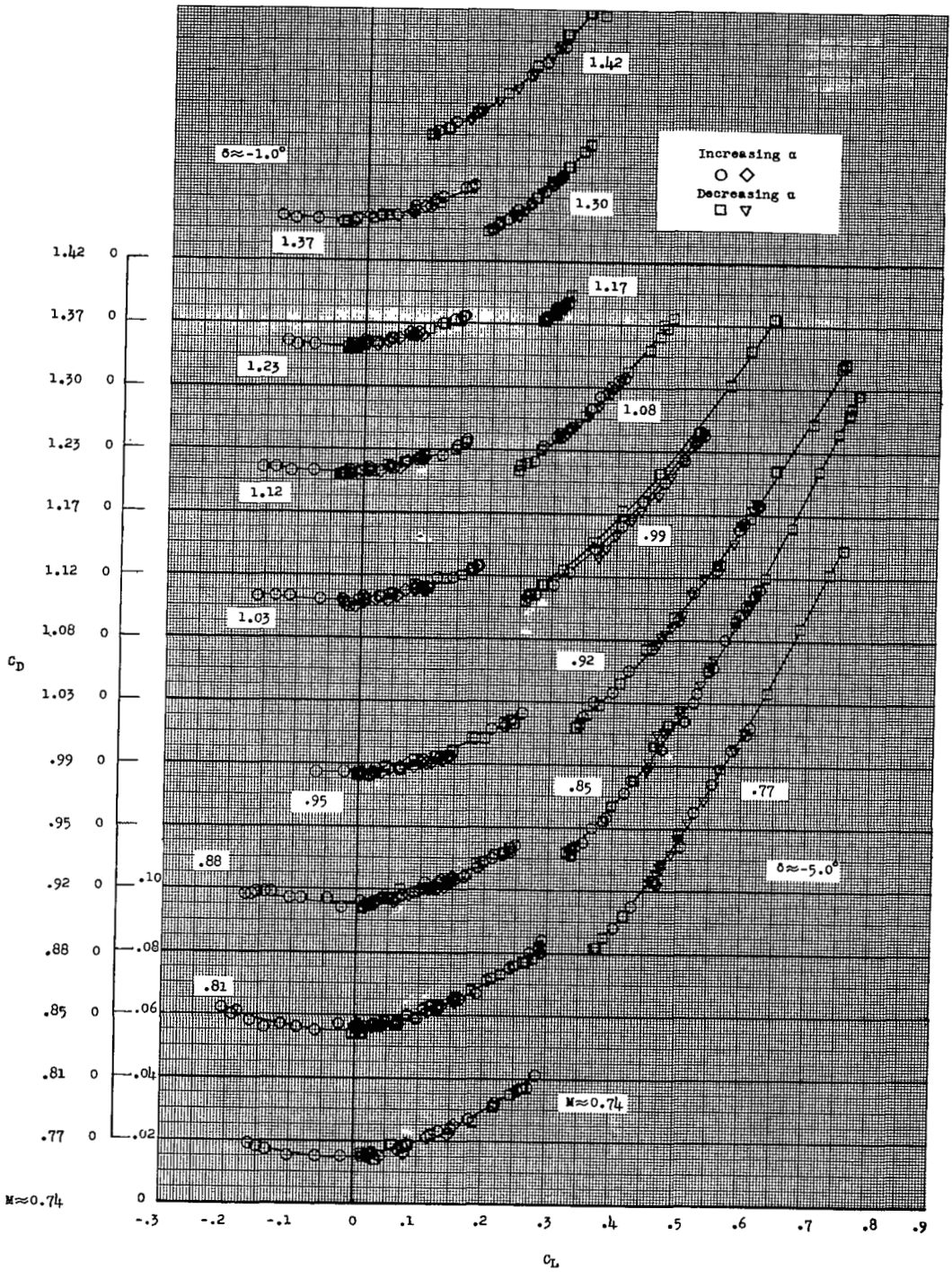

Figure 10.- Variation of drag with lift.

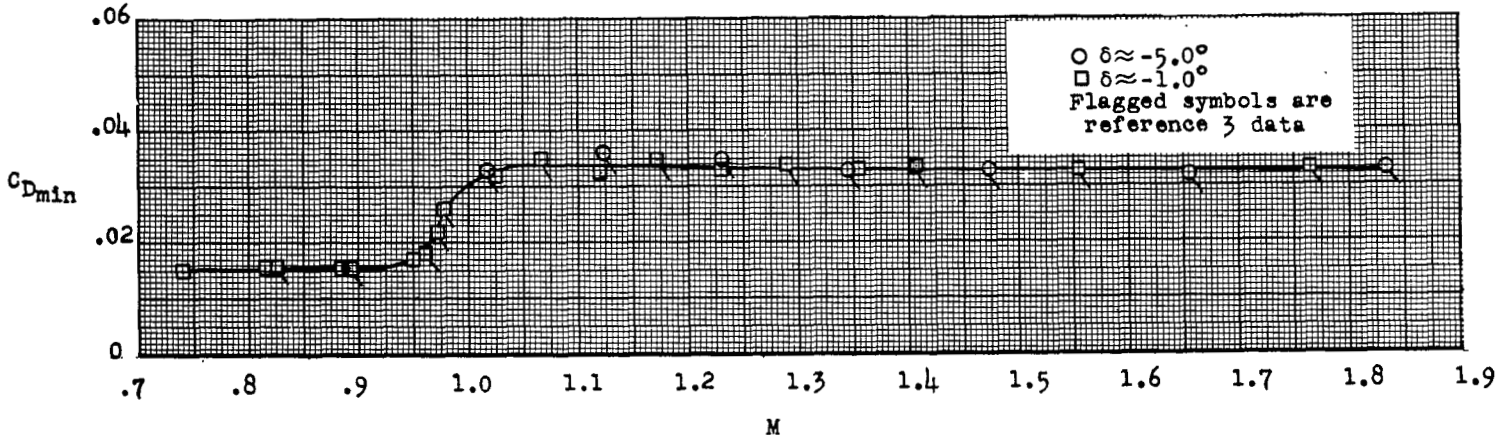

Figure 11.- Variation of minimum drag coefficient with Mach number.

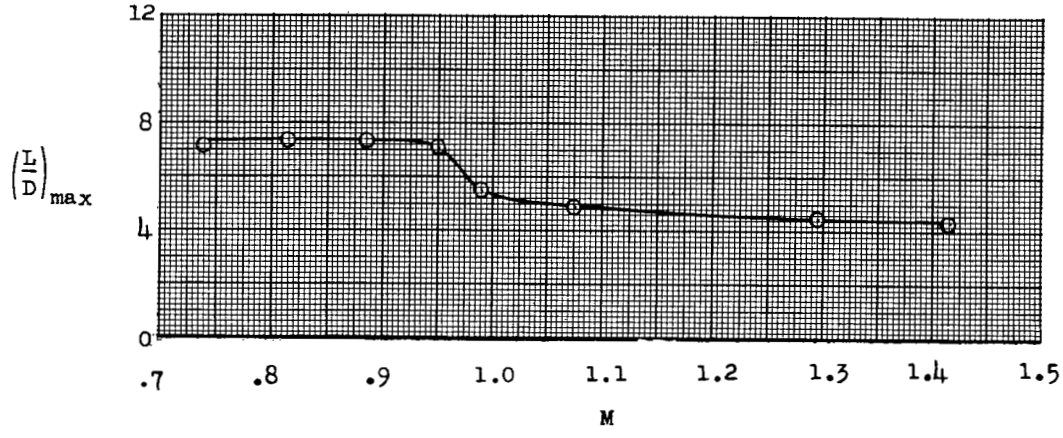

(a) Maximum lift-drag ratios.

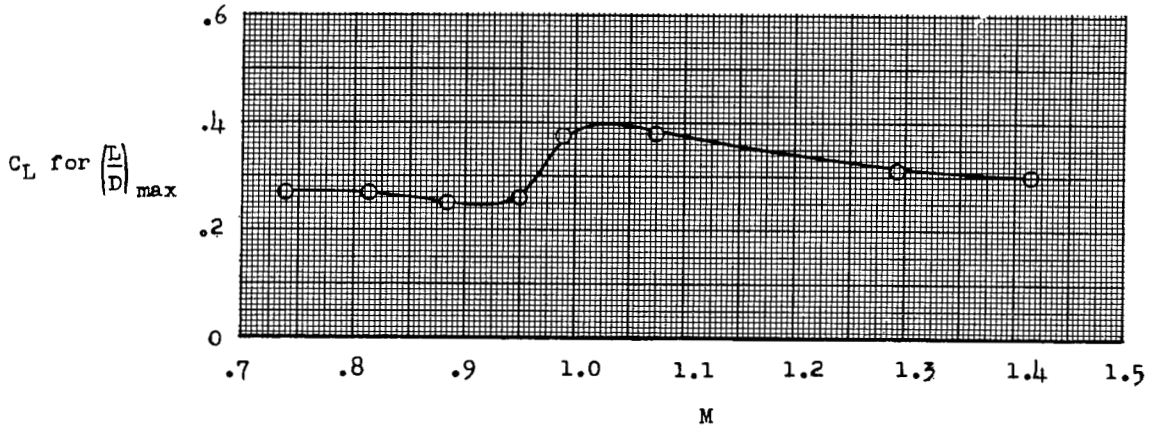

(b) Lift coefficients at which maximum lift-drag ratios occur.

Figure 12.- Variation of maximum lift-drag ratios and lift coefficients at which maximum lift-drag ratios occur as a function of Mach number.

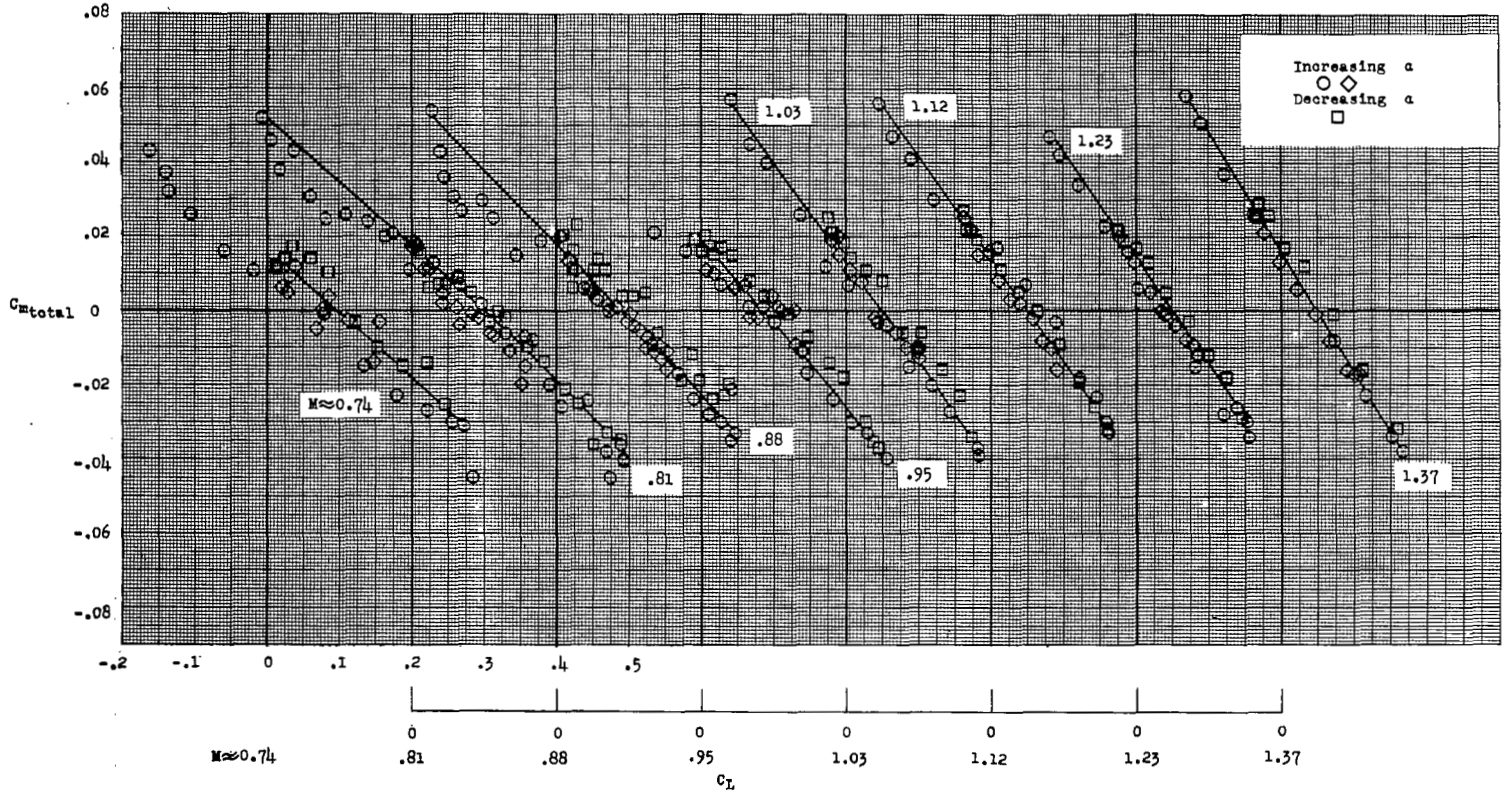

(a) $\delta = -1.0^{\circ}$.

Figure 13.- Variation of total pitching-moment coefficient with lift coefficient.

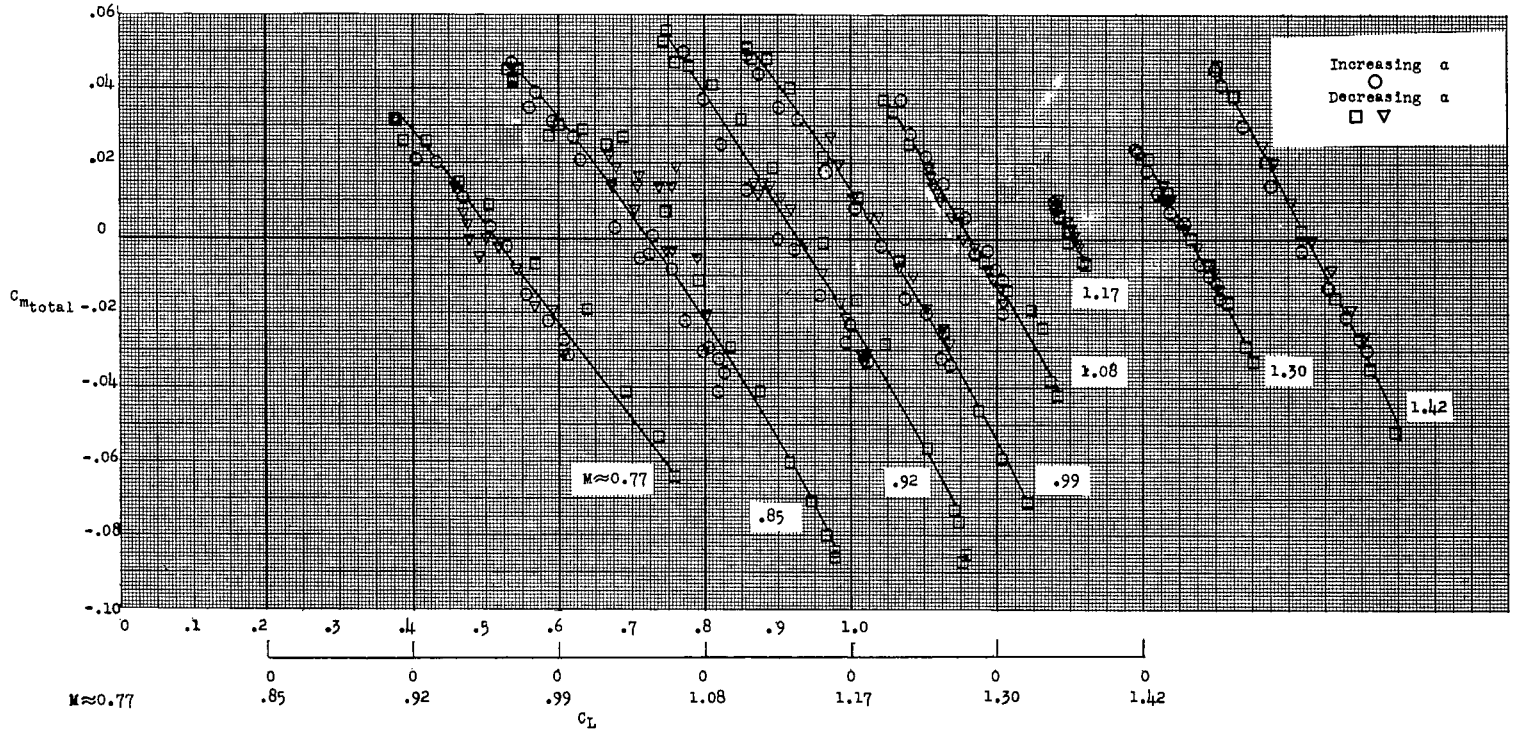

(b) $\delta = -5.0^\circ$.

Figure 13.- Concluded.

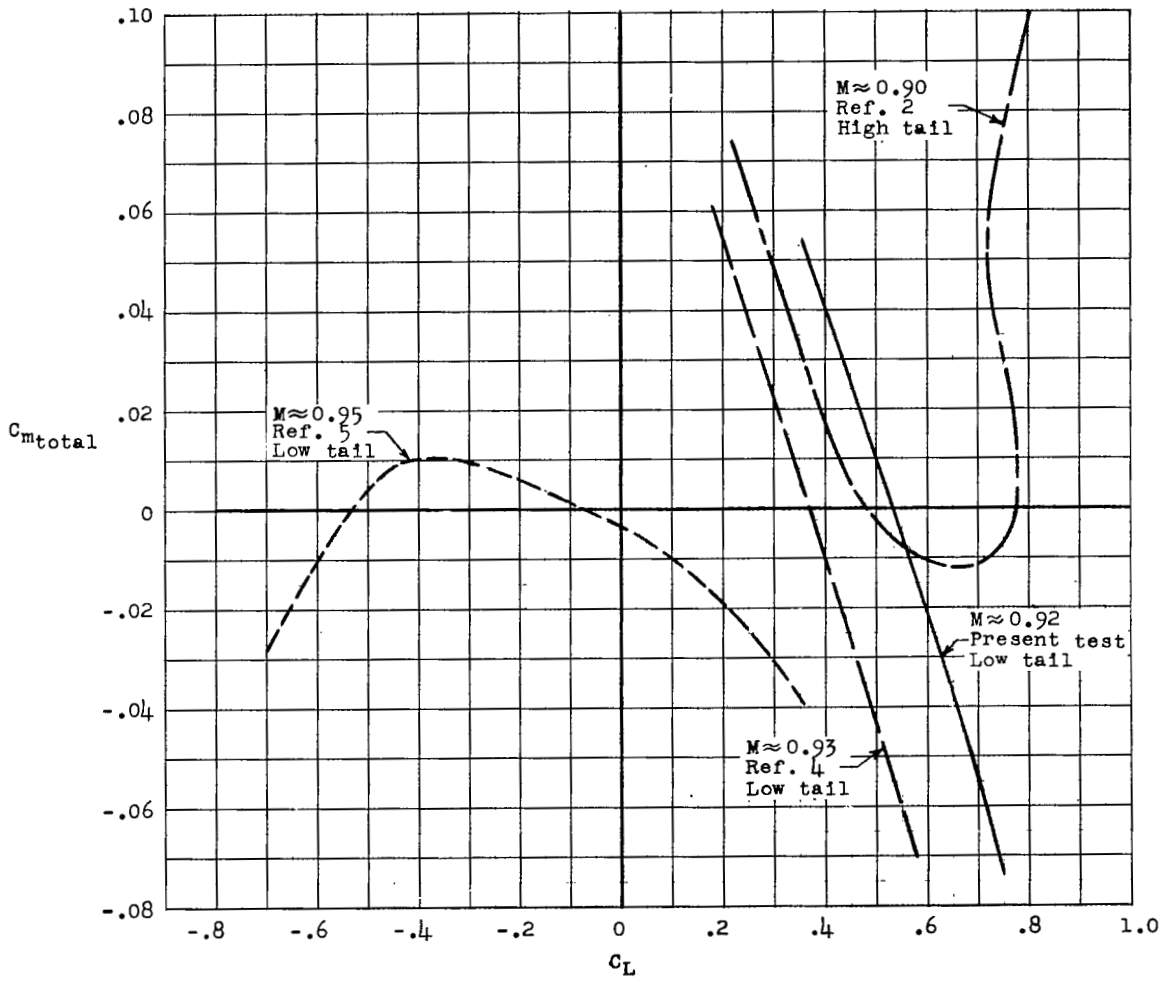

Figure 14.- Comparison of pitching-moment curves from various tests.

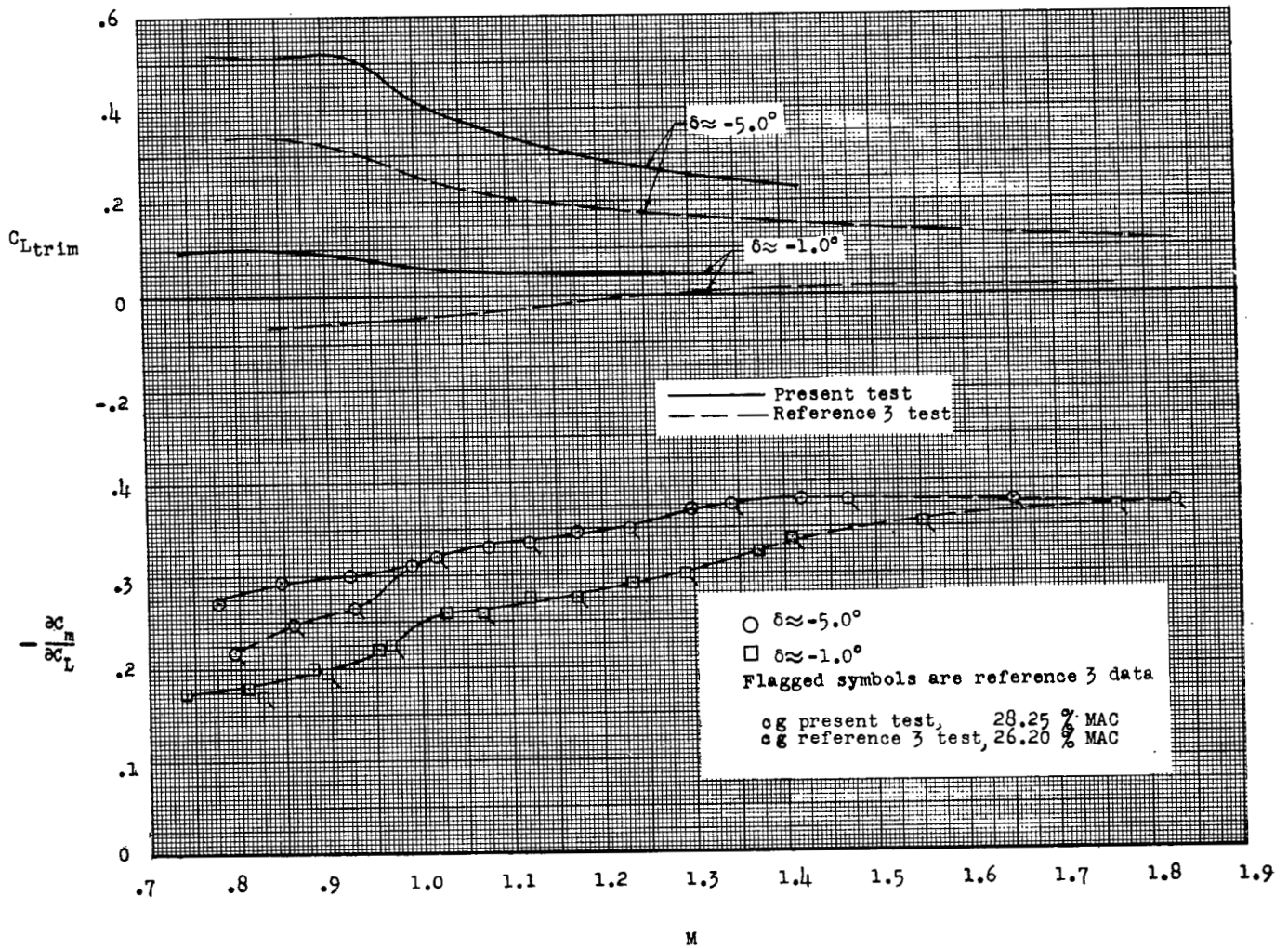

Figure 15.- Variation of static-stability parameter $\frac{\partial C_m}{\partial C_L}$ at trim conditions with Mach number.

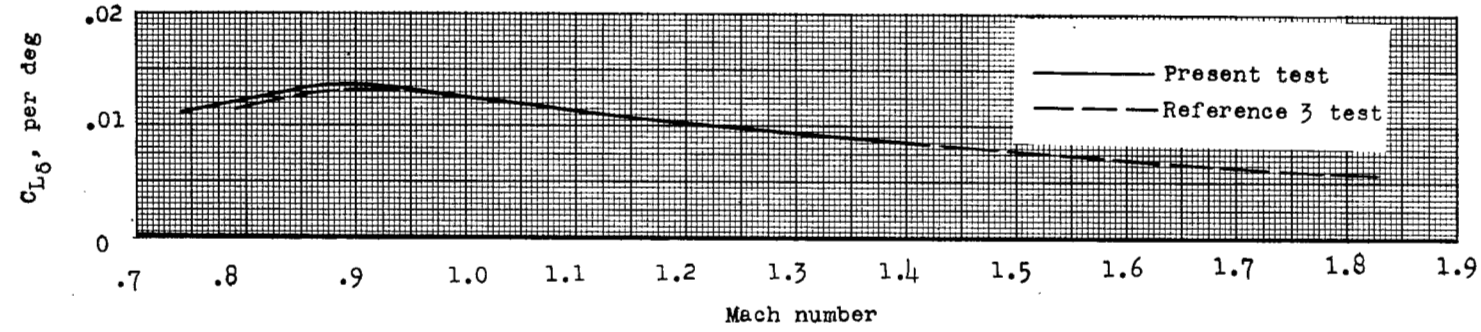

(a) Ability to produce lift.

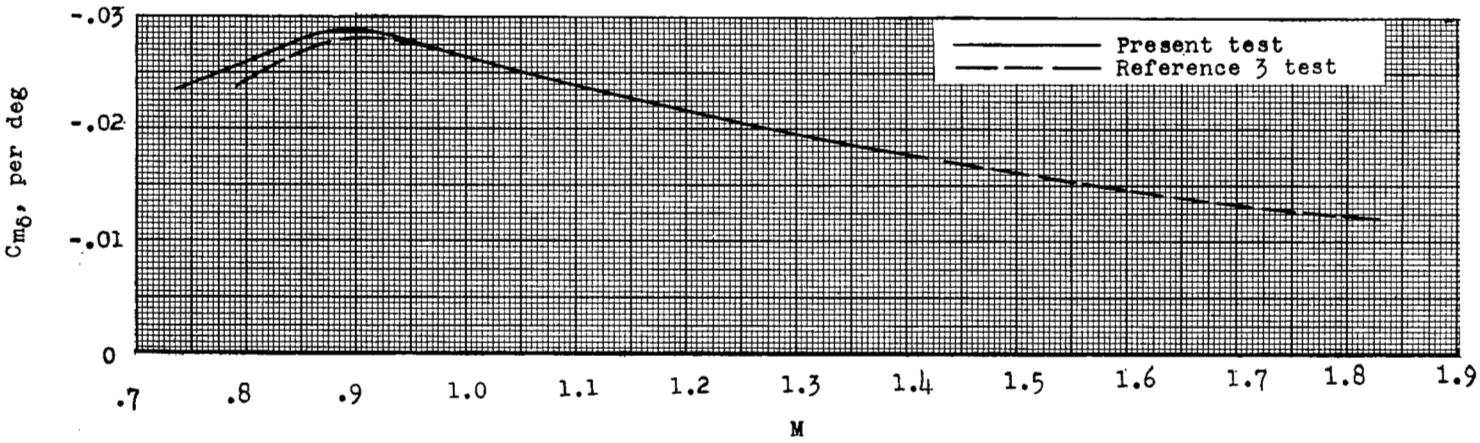

(b) Effectiveness in producing moment.

Figure 16.- Variation of ability of the horizontal tail to produce lift and effectiveness in producing moment with Mach number.

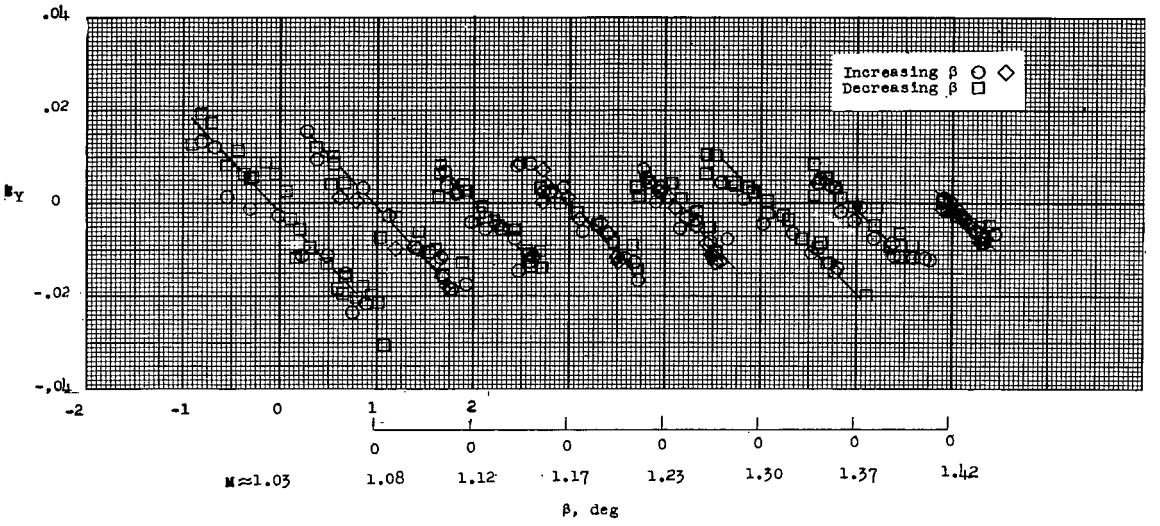

(a) Supersonic Mach numbers.

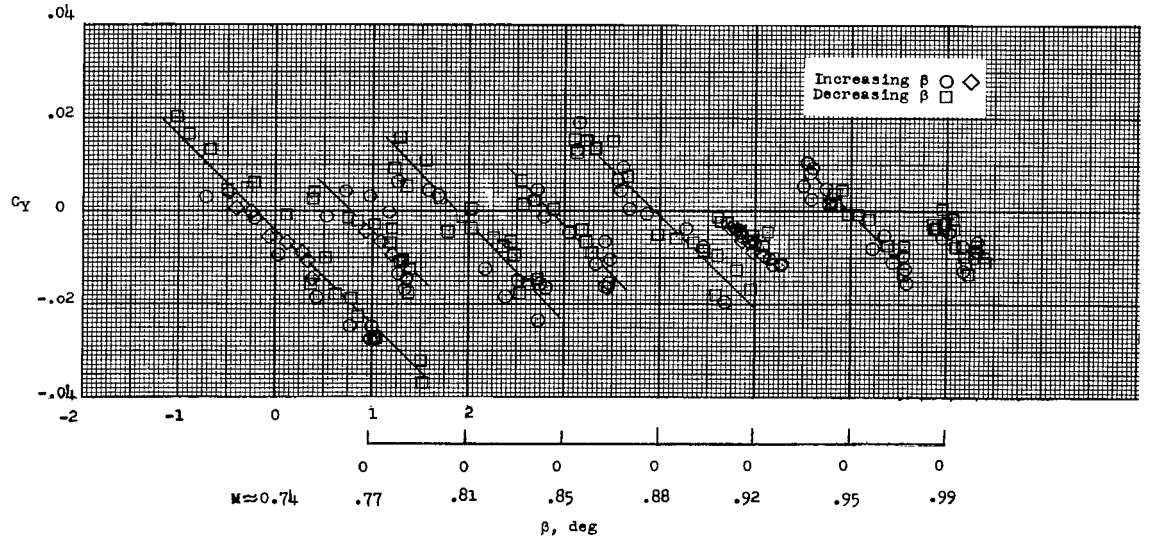

(b) Subsonic Mach numbers.

Figure 17.- Variation of side-force coefficient with angle of sideslip at supersonic and subsonic values of Mach number.

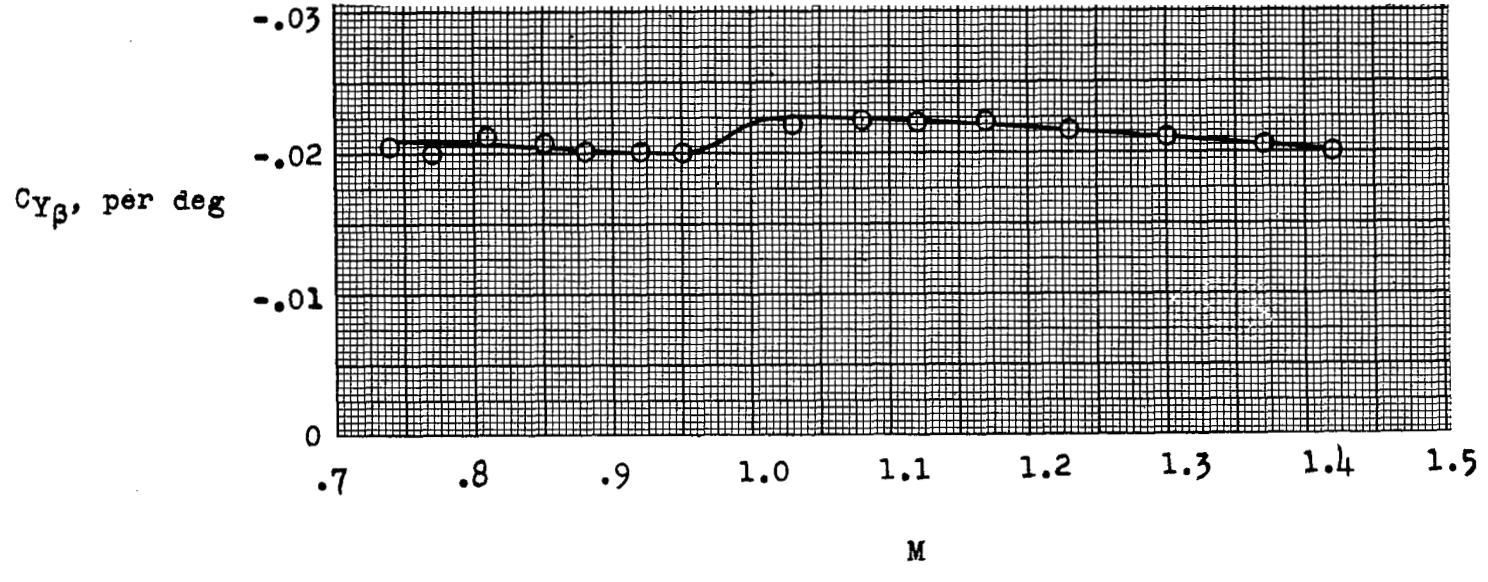

Figure 18.- Variation of C_{Y_β} with Mach number.

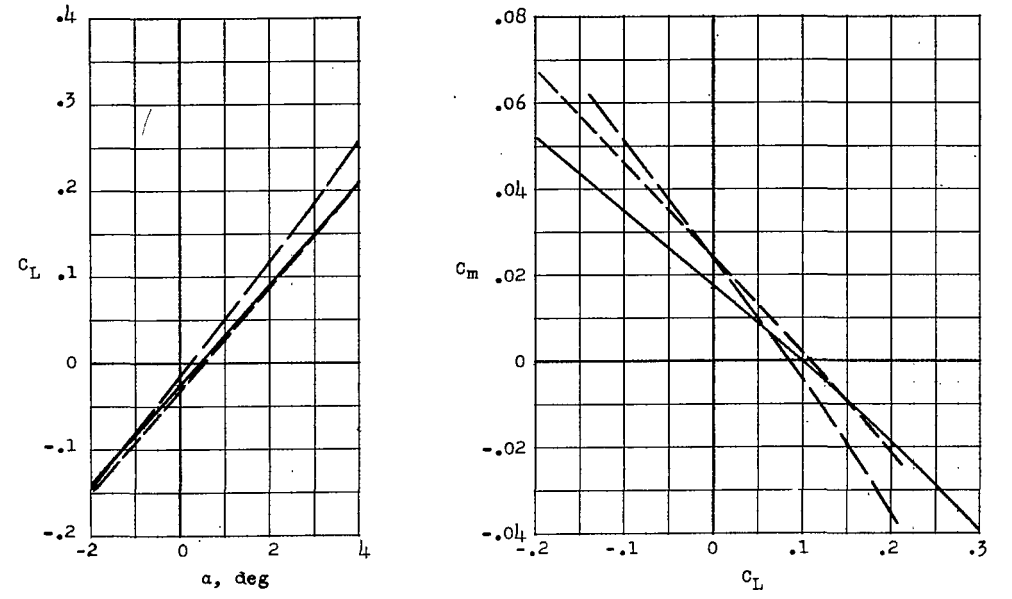

(a) M ≈ 0.80.

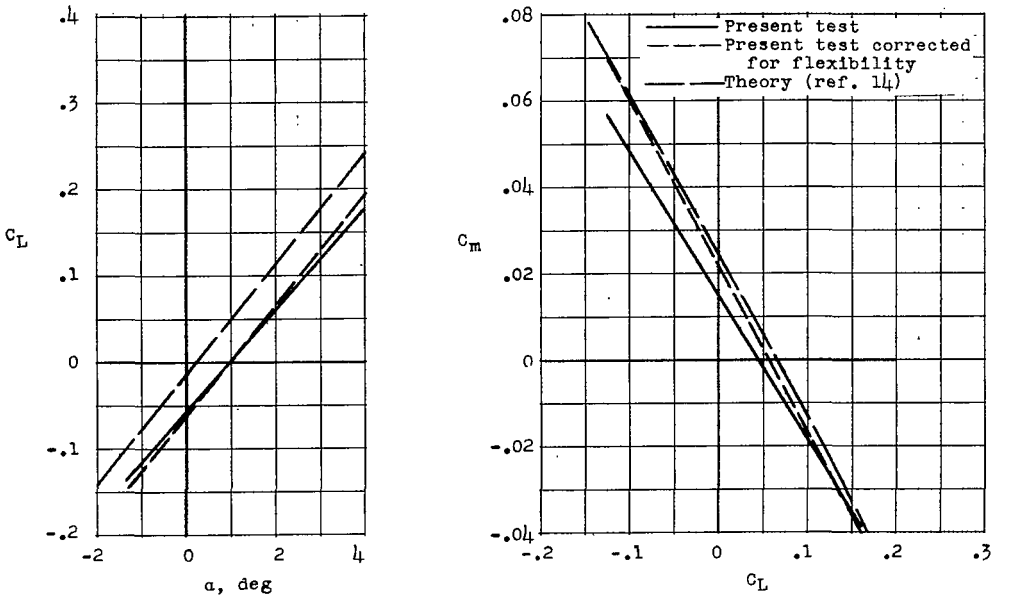

(b) M ≈ 1.40.

Figure 19.- Experimental and theoretical comparisons of lift and pitching moment.

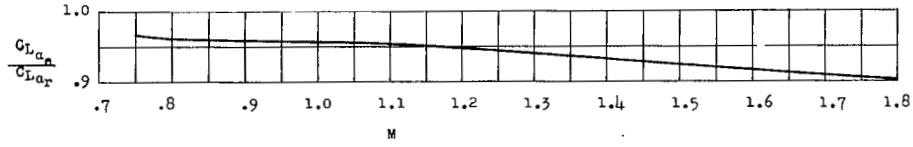

Figure 20.- Variation of elastic to rigid lift ratios as a function of Mach number.

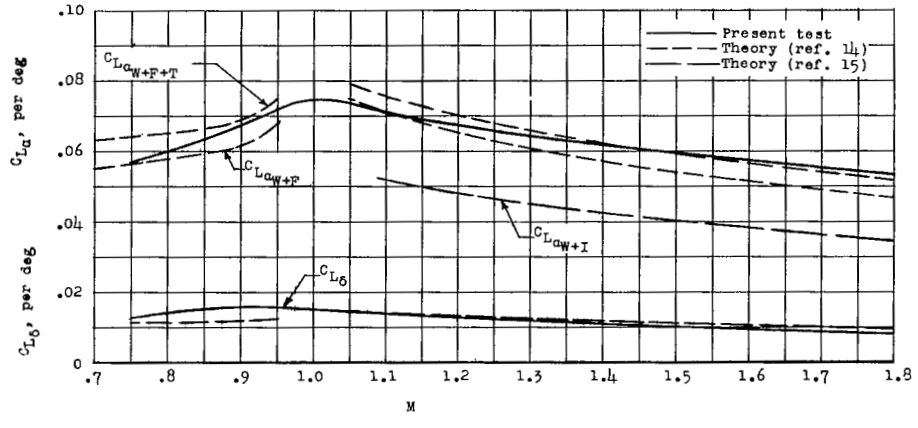

Figure 21.- Variation of theoretical and rigid experimental lift-curve slope and the ability of the horizontal tail to produce lift as a function of Mach number. $\delta \approx -1.0^\circ$.

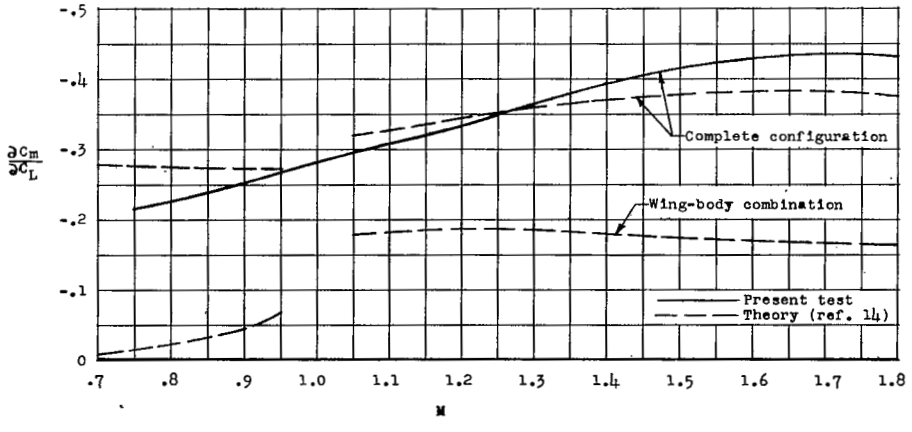

Figure 22.- Variation of theoretical and rigid experimental pitching-moment curves as a function of Mach number. $\delta \approx -1.0^\circ$.

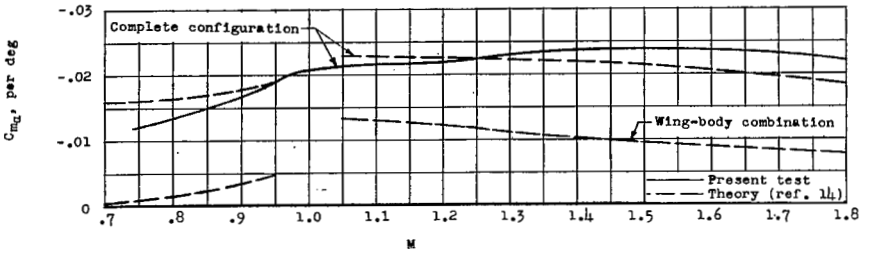

Figure 23.- Variation of theoretical and rigid experimental static longitudinal stability parameter C_{m_α} as a function of Mach number. $\delta \approx -1.0^\circ$.

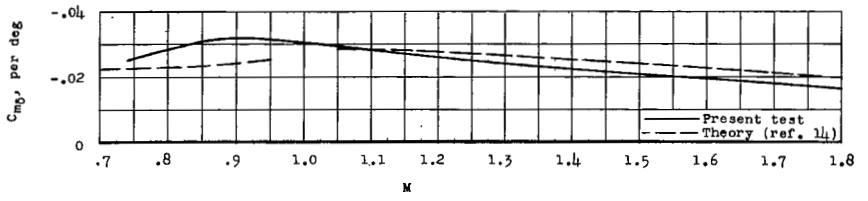

Figure 24.- Variation of theoretical and rigid experimental effectiveness of the horizontal tail to produce moment as a function of Mach number. $\delta \approx -1.0^\circ$.

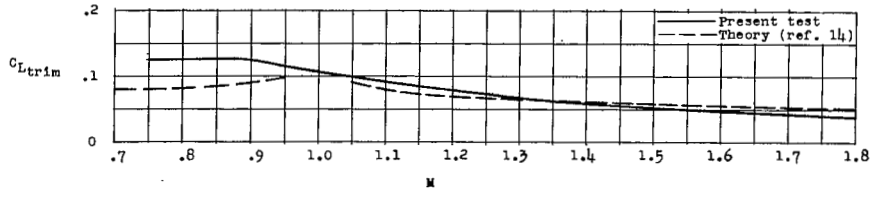

(a) Trim lift coefficient. $\delta \approx -1.0^\circ$.

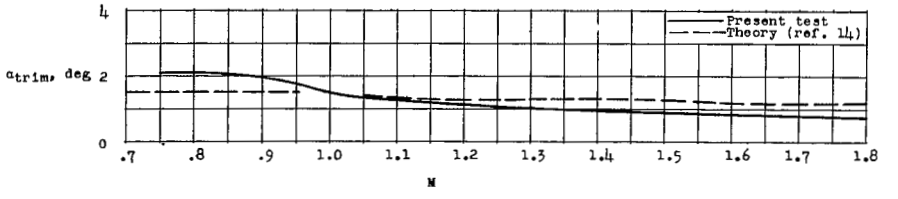

(b) Trim angle of attack. $\delta \approx -1.0^\circ$.

Figure 25.- Variation of theoretical and rigid experimental trim characteristics as a function of Mach number.

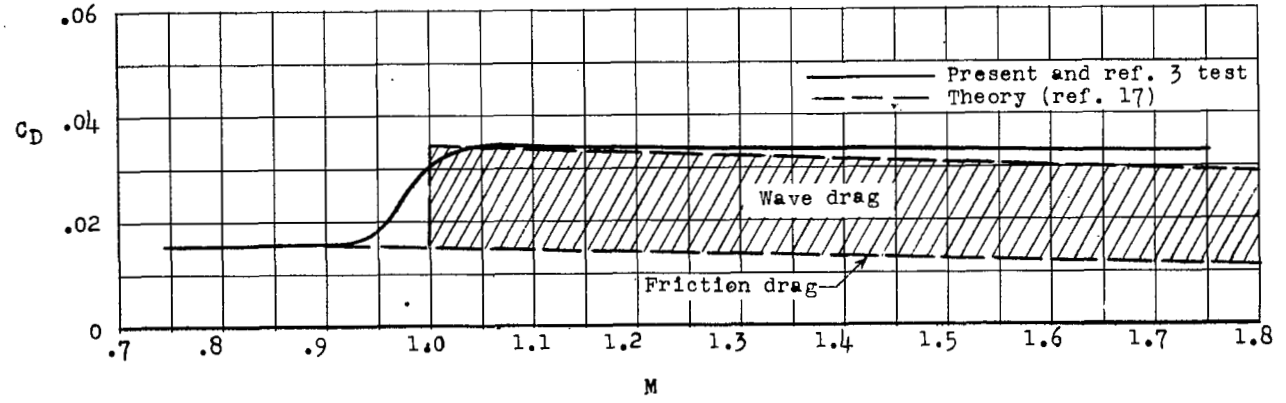

Figure 26.- Variation of theoretical and experimental drag coefficient with Mach number.

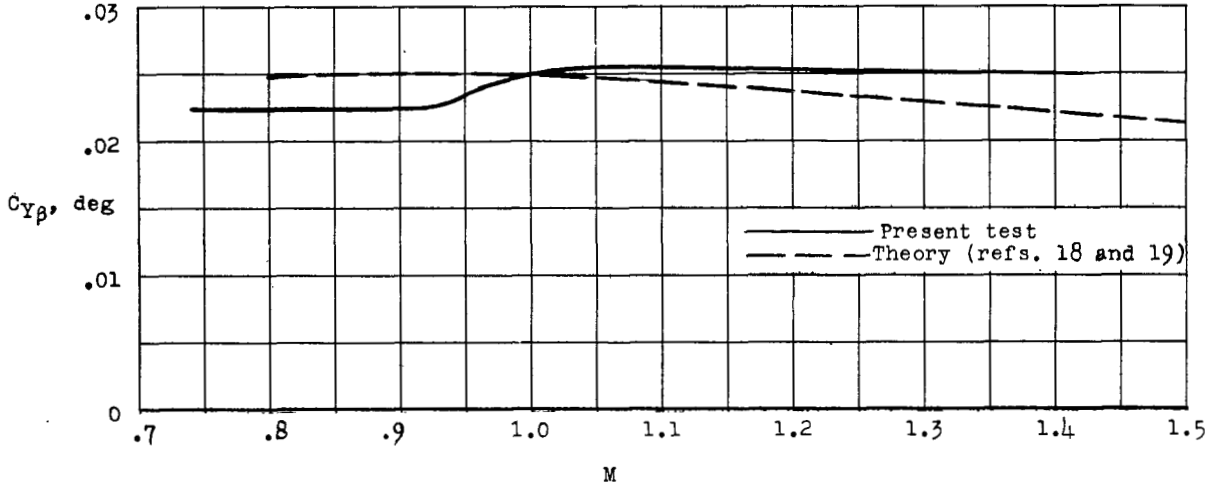

Figure 27.- Variation of theoretical and rigid experimental side-force derivative C_{Y_β} with Mach number for complete configuration.